This is a pre-print submitted to EarthArXiv.

This manuscript has been submitted to Basin Research, and undergone one round of peer review.

09.07.2025

Hothouse hydrology: Evolving river dynamics in the Eocene Montllobat and Castissent Formations, Southern Pyrenees

Jonah S. McLeod*[1,2], Alexander C. Whittaker[1], Gary J. Hampson[1], Rebecca E. Bell[1], Marine Prieur[3], Oliver G. Fuller-Field[1], Luis Valero[4], Xiang Yan[1], Jeffery M. Valenza[5]

1 Department of Earth Science and Engineering, Imperial College London, London SW7 2AZ, UK

2 Grantham Institute, Science and Solutions for a Changing Planet DTP, Exhibition Road, South Kensington, London SW7 2AZ, UK

3 Department of Earth Sciences, University of Geneva, 1205 Geneva, Switzerland

4 Departament de Dinàmica de la Terra i de l'Oceà, Faculty of Earth Science, University of Barcelona, Martí i Franquès s/n, 08028 Barcelona, Spain

5 Department of Geography, University of California, Santa Barbara, 1832 Ellison Hall, Santa Barbara, CA, 93106, USA

*Corresponding author: Jonah McLeod (jonah.mcleod18@imperial.ac.uk)

ACKNOWLEDGEMENTS

We thank Miguel Garces, an anonymous reviewer and Associate Editor Tian Yang for their constructively critical comments, which have improved the manuscript. This work was supported by the Natural Environment Research Council (grant NE/S007415/1) and Terrabotics (London). MATLAB (MathWorks) was used in our analyses.

ABSTRACT

Rivers are highly sensitive to climate and tectonic change, and understanding how fluvial systems respond to greenhouse climates in dynamic tectono-geomorphic settings is vital to projecting imminent landscape change in the face of global warming. We look to the southern Pyrenean Tremp-Graus basin during the Early Eocene Climatic Optimum (EECO), analogous to future anthropogenic climate scenarios. We focus on the fluvial deposits of the Montllobat and Castissent Formations, deposited during the early Pyrenean orogeny. This succession records a significant shift in geomorphology involving a 20 km progradation of the shoreline and its feeder rivers in < 0.8 Myrs. Using field-based quantitative palaeohydrology, we reconstruct the evolving morphometry and hydrodynamics of ancient river systems in a foreland basin. The transition from the Montllobat Formation into the Castissent Formation at c. 50.5 Ma is associated with a sharp change in palaeohydraulics: a statistically significant reduction in cross-set height, a 40% increase in water discharge, and a 15% increase in total sediment flux. This intensification in hydrological regime implies a clear climate driver, and is compounded with a switch in interpreted fluvial planform morphology from anastomosing to a dominantly braided planform at the onset of the Castissent interval, and a 1.4-fold increase in channel slope. We suggest the transient hydrological signature of the Castissent Formation was driven by Ypresian hyperthermal events superimposed on a levelling-off in the global cooling trend at the end of the EECO, and an increase in tectonic uplift rates at c. 50 Ma. This analysis holistically reconstructs the dynamics of ancient rivers in the Eocene Hothouse, and in conjunction with isotope and exhumation records, reveals the potential to extract complex tectono-climatic signals from fluvial stratigraphy.

Keywords

Sedimentology, stratigraphy, palaeohydrology, foreland basin, landscape dynamics

1 INTRODUCTION

Across Earth's history, landscapes and basins have responded to climate and tectonic forcings (Armitage *et al.*, 2011; Whittaker, 2012; Romans *et al.*, 2016). In today's warming world, multiple landscape systems are thought to be on the edge of marked geomorphic change (Flannigan *et al.*, 2006; Gariano & Guzzetti, 2016; IPCC, 2022; McLeod *et al.*, 2024) owing to increasing weather extremes worldwide (IPCC, 2022). In particular, rivers are one of the most significant drivers of landscape evolution (Romans *et al.*, 2016), transporting approximately 10^{10} tonnes of material across the Earth's surface each year (Milliman & Meade,

1983; Peucker-Ehrenbrink, 2009), and are documented to be highly sensitive to climate and weather patterns. While we cannot directly study landscape response to future climatic or tectonic change, we can collect observational data of geomorphic and sedimentary responses to past climate and tectonic change. Consequently, fluvial stratigraphy can be used as an archive of river response to past boundary condition change, meaning we can turn to the past to inform projections of future landscape change (Armitage *et al.*, 2011; Whittaker, 2012; Fielding *et al.*, 2018; Lyster *et al.*, 2020, 2022b; McLeod *et al.*, 2023; Sharma *et al.*, 2023; McLeod *et al.*, 2024).

Understanding the climate of the past has increasingly become possible in recent years using geochemical proxies of weathering, temperature and precipitation, mostly in marine settings but increasingly in the continental sedimentary record (e.g., Honegger *et al.*, 2020; Jaimes-Gutierrez *et al.*, 2024). Mountain belts are areas where rivers and continental processes may be particularly sensitive to climate change (IPCC, 2022), so the stratigraphic record of surface processes in mountainous regions could be especially valuable in deciphering the landscape dynamics of the past. Floodplain sediment and palaeosols already present a useful repository of these preserved environmental signals on the continents (e.g., Honegger *et al.*, 2020). However, river channels are more dynamic settings, and whilst they do record landscape change, disentangling climatic from tectonic information is challenging, and this is the focus of ongoing research (Armitage *et al.*, 2011; McLeod *et al.*, 2023, 2024; Sharma *et al.*, 2023; Prieur *et al.*, 2025; Rezwan *et al.*, 2025).

Facies-based sedimentological analysis of fluvial stratigraphy can yield important insights on the behaviour of ancient rivers in response to external drivers (Plink-Bjorklund, 2015; Colombera *et al.*, 2017; Fielding *et al.*, 2018; McLeod *et al.*, 2023; Boyrie *et al.*, 2025). However, robust quantitative constraints on palaeohydrology are essential for extracting detailed insights on the sensitivity of landscapes to climate and tectonic change, and in doing so, using the past to inform understanding of landscape change in the present and future. There is a growing wealth of techniques available for reconstructing the hydrology of rivers in the geologic past (Parker, 1976; Leclair & Bridge, 2001; Trampush *et al.*, 2014; Bradley & Venditti, 2017; Chamberlin & Hajek, 2019; Long, 2021; Lyster *et al.*, 2023; Wood *et al.*, 2025), many of which are based on measurements of primary geologic observables in stratigraphy such as grain-size, bedform size and preservation (e.g., dune cross-set thicknesses), and stratigraphic architecture (e.g., to reconstruct channel morphology and migration). Scaling relations developed by Bradley & Venditti (2017) and Leclair & Bridge (2001) based on field

and laboratory data, as well as theoretical considerations, permit reconstruction of river flow depths from dune-cross-sets. Experimental insights on bedform evolution (e.g., Das et al., 2022) present opportunities to interpret flow stage from preserved river deposits. Lyster *et al.* (2022a) built on Parker's (1976) use of planform (plan-view morphology) stability fields to constrain river planform geometry using quantitative palaeohydrologic reconstructions in the rock record, with new comparisons to modern river datasets. Advances such as these are expanding our capacity for extracting environmental signals from ancient geomorphic systems (Castelltort & Van Den Driessche, 2003; Allen, 2008; Romans *et al.*, 2016b; Jerolmack & Paola, 2010; Lyster *et al.*, 2022b).

In this paper we address the challenge of extracting competing climatic and tectonic signals from fluvial channel-fill strata, specifically in a hothouse environment. We use quantitative geologic techniques to reconstruct the evolving morphometry, transport dynamics and planform style of the well-documented Castissent and Montllobat formations located in the Pyrenean mountains of Spain for the first time, and we compare them to modern river systems and those preserved in stratigraphy. In particular, we aim to use the dynamic channel-fill deposits of ancient rivers to shed new light on the response of fluvial hydrology to environmental and/or tectonic signals in the past, and to reconstruct the sensitivity of palaeo-landscapes to known boundary condition changes. In doing so, we capture the geomorphic response of ancient rivers to the evolving climate and tectonics of the early Pyrenean orogeny during the hottest period of the Cenozoic (Westerhold *et al.*, 2020; IPCC, 2022).

2 GEOLOGIC BACKGROUND

The fluvial successions of the lower Eocene in the south-central unit of the southern Pyrenees of Spain offer extensive outcrop exposure within the dynamic setting of the growing Pyrenean orogen (e.g., Cabello et al., 2018; Marzo et al., 1988; Nijman & Puigdefàbregas, 1977), and record fluvial deposition during the Early Eocene Climatic Optimum (EECO), a global greenhouse period which represents the climax of the 9 million-year-long Eocene Hothouse (Winnick *et al.*, 2015; Westerhold *et al.*, 2018; Broz *et al.*, 2024). There are also a number of hyperthermal events superimposed on the EECO – these represent brief periods of pronounced global warming, considered anomalous when compared to typical conditions during this time interval.

During the early Pyrenean orogenesis, runoff flowed south into foreland sub-basins bound by imbricate thrusts, and rivers deflected westwards where they deposited a wedge of fluvio-

deltaic, clastic sediment known as the Montanyana Group (Nijman & Nio, 1975). The best preserved units in the Montanyana succession are the Lower and Middle Montanyana Groups (LM, MM, Nijman, 1998), and in the fluvial domain (Tremp-Graus Basin) these comprise the Montllobat (Mlb) and Castissent (Cst) Formations (Ypresian, c. 53.0 – 49.7 Ma), respectively (Fig. 1). The rivers of the Montllobat and Castissent Formations deposited continental sediment NW into an elongate bay, connected to the Atlantic (Juvany *et al.*, 2024), forming the Montanyana delta. The later Upper Montanyana Group (UM) sediments are similar in facies to the LM Group (Nijman, 1998).

The Montllobat (c. 53.0 – 50.5 Ma) and Castissent (50.5- 49.7 Ma) formations crop out across the Spanish Pyrenees in the Tremp-Graus basin in Catalonia and Aragon, and have been the focus of sedimentological and stratigraphic investigation since the mid-1970s (e.g., Nijman & Nio, 1975; Nijman & Puigdefàbregas, 1977). The Castissent Formation forms a regional marker unit with a total thickness of 50 – 100 m and represents a strong progradational episode, which saw the shoreline and rivers of the clastic wedge prograde 20 km over the underlying Montllobat Formation (and its shallow marine equivalent, the Castigaleu Formation) for an estimated duration of 800 kyrs (Honegger *et al.*, 2020). Due to this distinctive progradation, excellent outcrop preservation, and its use as a reservoir analogue including its down-system genetic equivalents (e.g., Clark & Pickering, 1996; Puig *et al.*, 2019), the sandstones of the Castissent Formation have received more focus than other units in the continental Montanyana Group. It has been suggested that this progradation could be attributed to an increase in hinterland exhumation rate (Whitchurch et al., 2011; Curry et al., 2021; Fig. 2) and/or a possible change in climate or sea-level (Nijman, 1998; Honegger *et al.*, 2020).

The climate of the Castissent interval in particular is becoming increasingly well-constrained, as Honegger at al. (2020) used isotopic and geochemical signatures preserved in floodplain sediment and palaeosols to identify climate change during a hyperthermal event recorded within the formation. They identified a carbon isotopic excursion (CIE) at c. 50 Ma as Eocene hyperthermal "U" (Fig. 2), associated with enrichment in immobile Ti, Zr and Al. Based on the CaO/Al_2O_3 ratios of the bulk palaeosol material, the average climate is reconstructed as sub-arid with a mean annual precipitation (MAP) of 376 mm/a, increasing to as high as 754 mm/a during CIEs. $\delta^{13}C$ records of benthic carbonates (Westerhold *et al.*, 2017; Honegger *et al.*, 2020) also show that Castissent deposition coincides with a levelling-off in a long-wavelength trend of global cooling (Fig. 2). Insights like this are helping to elucidate changing climate

156 towards the end of the EECO, and suggest Montllobat and Castissent rivers were subject to
157 tectono-climatic perturbations that have geologic preservation potential.

158 Marzo et al. (1988) mapped and logged the Castissent Formation in some detail and described
159 three multistorey sandsheet complexes, each described as a member of the Castissent
160 Formation (Fig. 3A). These sandsheet complexes are attributed to three successive fluvial
161 systems separated by marine incursions and preserved floodplain deposits. Nijman (1998)
162 identified the Castissent Formation as equivalent to the Middle Montanyana (MM)
163 Megasequence, containing three Sequences (MMI, MMII and MMIII) which correspond to
164 Castissent Members A, B and C (Marzo et al., 1988), respectively. Channel-fill bodies are
165 vertically and laterally amalgamated, sand-rich and have a distinctive white-weathering and
166 rounded exposure pattern (Fig. 4D-E). The Castissent has previously been interpreted as a
167 braided system due to its sheet-like and predominantly multistorey, multilateral architectural
168 style (Nijman & Nio, 1975). It is correlated westwards with the deep-water turbidites of the
169 Arro and Fosado Formations in the Ainsa Basin (Mutti & Sgavetti, 1987) and tentatively with
170 the Torla and Broto systems in the Hecho Group of the Jaca basin (Caja *et al.*, 2010; Cornard
171 & Pickering, 2020).

172 Whilst the Castissent interval lasted c. 0.8 Myrs, the underlying Montllobat Formation formed
173 over approximately 2.5 Myrs, and represents the first major phase of NW-oriented fluvial
174 drainage in the Pyrenean foreland. The Montllobat Formation comprises variably isolated and
175 amalgamated, channelised sandstone and conglomerate bodies encased in mudstone-
176 dominated, mottled floodplain deposits (Cabello *et al.*, 2018) with a total thickness of 150 –
177 250 m. The Montllobat Formation has been interpreted to contain deposits of both meandering
178 rivers with prominent point-bar deposits (Van Eden, 1970; Nijman & Nio, 1975; Cabello *et al.*,
179 2018), and sheetflood-dominated river systems (Van der Meulen, 1989). The Lower
180 Montanyana Group (Montllobat Formation) comprises two Megasequences, the Lower LM
181 (LLM) and Upper LM (ULM), separated by a Megasequence boundary associated with
182 southward progradation of coarse-grained alluvial fan deposits and an extensive conglomerate
183 unit (Nijman, 1998). This boundary is mapped by the Catalan geologic survey (ICC) on their
184 Espills (1:2500; 251-2-2) sheet as conglomerate unit C3 (Picart *et al.*, 2010). We treat this
185 Megasequence boundary as the boundary between two members of the Montllobat Formation,
186 which we describe here as Montllobat A (MlbA) and Montllobat B (MlbB).

Figure 3A summarises the stratigraphic framework used for this work: the Montllobat Formation is equivalent to the LM Group, and its two Megasequences (LLM and ULM) are here labelled as Members MlbA and MlbB, respectively. The Middle Montanyana (MM) Group comprises one Megasequence, the Castissent Formation, and is subdivided into Members CstA, CstB and CstC (Marzo et al., 1988), each representing individual cycles within the MM Megasequence as defined by palaeosol formation and repeated phases of aggradation and degradation (*sensu* Nijman, 1998). See Table S1 for further explanation.

These units are stratigraphic exemplars of the interplay between climate and tectonics in ancient geomorphic systems: hyperthermal events superimposed on a long-term cooling trend from the EECO competed with tectonic change in the early Pyrenees. High-frequency climate signals are becoming more widely interpreted in the continental rock record (McInerney & Wing, 2011; Turner, 2018; Rush *et al.*, 2021; Prieur *et al.*, 2025), including in the Castissent Formation, where indicators of climate change are preserved in floodplain sediment (Honegger at al., 2020). These units offer an excellent opportunity to quantify palaeohydraulic changes in a well-defined tectonic and climatic context

3 METHODS

3.1 Field Data

Field data were collected at 42 sites in the Castissent and Montllobat formations (Fig. 1). Primary numerical field observations (Fig. 4) included grain-size, the thickness and lee face orientation of cross-sets, and the thickness, length, and accretion orientation of barforms. These primary field observations were collected in the context of previous analyses of facies and stratigraphic architecture in the Castissent and Montllobat formations (Marzo *et al.*, 1988; Nijman, 1998; Cabello *et al.*, 2018; Puig *et al.*, 2019). Our field methodological approach for reconstructing palaeohydrology follows a workflow which has been tested in various geologic settings recently (e.g., Ganti et al., 2019; Lyster et al., 2020; Wood et al., 2022) and is summarised below.

Cross-sets, the preserved remnants of river dunes, can be generally expected to scale in size with river flow depth (e.g., Bradley & Venditti, 2017) with some caveats which we discuss below – see *Flow Depth*. To estimate mean cross-set thickness, h_{xs}, from fluvial deposits, which are used in our reconstructions below, we obtained full thickness distributions from 1553 thickness measurements across 147 cross-sets, by measuring thickness along the major axis of

a cross-set at 10-15 regular intervals (with a mean of N = 10.6 measurements per cross-set, cf. Lyster et al., 2022; McLeod et al., 2023). A scaling factor between maximum and mean cross-set thickness was calculated based on these data, so that our larger data set of maximum cross-set thicknesses in the two formations could be incorporated within our analysis (N = 1539) by downscaling to estimated mean thicknesses. Accordingly, combining our measured and downscaled datasets, we used N = 1686 cross-set thickness measurements for palaeohydrological reconstruction across the Montllobat and Castissent formations.

Where cross-set thickness distributions were obtained, we also measured median grain-size (D_{50}) and lee face orientation. Where grains were < 2 mm in diameter, D_{50} was estimated (N = 147) using the scheme of Wentworth (1922), and in conglomeratic bodies in which $D_{50} \geq 2$ mm, grain size distributions were measured (N = 22 distributions of 100 grains each) according to the point-count method of Wolman (1954)), allowing reconstruction of maximum formative flow conditions according to average bedload material grade. Cross-set lee face orientations (N = 856) were measured and restored to palaeo-horizontal using measurements of regional structural dip in Stereonet 11 (Allmendinger *et al.*, 2013). Restored lee face measurements were used in reconstructions of palaeocurrent direction and planform morphology.

Preserved barforms were recognised in the field by their sloping bar-accretion surfaces, often accompanied by superimposed dune-scale cross-stratification, following the approach of Chamberlin & Hajek (2019). The heights of barform accretion sets (h_{acc}, Table 1) and channel-fill bodies (N = 221) were measured using a TruPulse laser range finder to provide further constraints on palaeoflow depth. Barform accretion surface orientations (N = 703) were measured using the same methodology as cross-set lee faces in order to determine accretion direction and bar mode – whether bars migrate downstream, laterally, or upstream relative to flow direction – sampling accretion surfaces at their steepest dip angle relative to the structural dip of bedding.

3.2 Analytical Workflow

Primary field data were processed using a quantitative palaeohydrological workflow based on a suite of theoretical-numerical models, experimental relations and field observations. This methodological workflow is summarised in Figure 5. All uncertainty has been propagated through this workflow using Monte Carlo simulations with 10^6 runs, incorporating random distributions between uncertainty limits, following established methods (Ganti *et al.*, 2019;

Lyster *et al.*, 2021; McLeod *et al.*, 2023). To estimate cross-set thickness, flow depth, channel gradient, flow velocity, and unit water and sediment flux, rectangular (uniform) uncertainty distributions were used (see Supplemental Material for extended methodology). This weights all uncertainty equally and avoids introduction of additional assumptions (cf. Lyster *et al.*, 2021). In channel width estimates, we employed triangular uncertainty distributions in some cases, as explained further below.

Cross-set Thickness

The primary palaeohydrological reconstruction available from cross-sets is the height of the original dune, h_{d}. This was estimated using the relation of Leclair & Bridge (2001) that mean cross-set thickness (h_{xs}) is, on average, around 1/3 of the original dune height:

$$h_{\mathrm{d}} = C h_{\mathrm{xs}} , \tag{1}$$

Where C is a bedform preservation ratio with a value of 2.9 ± 0.7, derived from observational river datasets and experimental flumes. This formula is rooted in the theoretical model developed by Paola & Borgman (1991) for dune migration over random topography on the bed with a low angle of climb, assuming the dunes are in equilibrium with the prevailing flow conditions. This model has been used to elucidate original dune height from stratigraphy in a range of geologic settings (Ganti *et al.*, 2019; Lyster *et al.*, 2021; McLeod *et al.*, 2023).

Flow Depth

Flow depth is an important metric in understanding the dynamics of ancient river systems. We used two approaches to estimate flow depth: a bedform approach, and a barform approach. The bedform approach uses the dataset of h_{d} in the relation of Bradley & Venditti (2017) to obtain an estimate of median formative flow depth, H:

$$H = x h_{\mathrm{d}} , \tag{2}$$

where x is a scalar based on a compilation of flow and dune dimension data. The relative heights of flow depth and dunes and cross-sets depends on flow stage (Das *et al.*, 2022), so uncertainty is represented in the scalar x, which has an interquartile range between 4.4 and 10.1, and a median value of 6.7 (Bradley & Venditti, 2017). The results of this approach can be independently compared with barform data, using the thickness of bar accretion sets as robust architectural constraints on flow depth (Das *et al.*, 2022). These represent minimum bounds on

bankfull flow depth, since barforms with measurable accretion surfaces have thickness equal to a minimum flow depth in formative conditions. Moreover, barform accretion packages are rarely fully preserved in fluvial strata, so reconstructed flow depths using the barform approach represent conservative minima. We do not consider compaction to have affected measured thickness of cross-sets or accretion sets, since it often has a relatively minor influence on sandstone-dominated units, and mostly when grain crushing occurs or when the initial sediment has anomalously high porosity or low proportions of intergranular cement (Fisher *et al.*, 1999).

Palaeoslope

Channel palaeoslope, S, was reconstructed using the approach of Trampush et al. (2014) based on empirical data rooted in hydrological theory, and is appropriate for the range of grain-sizes observed in the Montllobat and Castissent Formations, including suspended, mixed and bedload rivers. S (in units of m/m) is given by:

$$logS = \alpha_0 + \alpha_1 logD_{50} + \alpha_2 logH\,, \tag{3}$$

where α_0, α_1 and α_2 are constants given as -2.08 ± 0.036, 0.254 ± 0.016 and -1.09 ± 0.044 respectively, and D_{50} is the median grain-size.

Flow Velocity and Unit Water Discharge

The formula established by Manning et al. (1890) was used to estimate water flow velocity, U:

$$U = \frac{1}{n} H^{\frac{2}{3}} S^{\frac{1}{2}}\,, \tag{4}$$

where n is a roughness coefficient approximated as 0.03 (Lyster *et al.*, 2020). U, with units of m/s can be multiplied by flow depth to estimate the unit water discharge, q_w, in units of m^2/s: $q_w = UH$.

Sediment Flux

Reconstructing sediment flux through rivers is essential to understand their erosive and transport power: rates of sediment flux are highly sensitive to changing climate and tectonics (Sharma *et al.*, 2023; McLeod *et al.*, 2024; Prieur *et al.*, 2025; Rezwan *et al.*, 2025), and can inform about landscape dynamics from source to sink in the past. In this study, we tested several estimators of sediment flux, and base our results on the total load predictor of Engelund &

Hansen (1967) for sand-dominated deposits and the bedload predictor of Meyer-Peter & Müller (1948) for gravel-dominated deposits. The relation of Engelund & Hansen (1967) gives sediment flux per unit width, q_s, in units of m^2/s for sand-grade deposits as:

$$q_s = q_t^*(RgD_{50}^3)^{0.5} \quad , \tag{5}$$

where R is the submerged density of sediment (~1.65 for quartz), g is 9.81 m/s^2, and q^*_t is the dimensionless Einstein number, relating shear stress and bed friction (see Supplemental Material for extended methodology). For gravel-dominated channel deposits, we calculated unit bedload sediment flux using the formula of Meyer-Peter & Müller (1948) modified by Wong & Parker (2006):

$$Q_{s,bf} = \left(g\ {D_{50}}^{\mathbf{3}}\ \Delta\rho\right)^{0.5} C(\tau_{*b} - \tau_{*c})^{\alpha} \quad , \tag{6}$$

where Δρ is the dimensionless submerged specific gravity of sediment (1.6); dimensionless basal shear stress τ_{*b} is given as

$$\tau_{*b} = H_{bf}S\ /\Delta\rho D_{50} \ , \tag{7}$$

and dimensionless critical shear stress τ_{*c} and constants C and α are taken as 0.047, 4.93 and 1.6, respectively, after Wong & Parker (2006).

Channel Width

Estimating the width of active flow from stratigraphic deposits has been a continuing challenge in the field of fluvial geology. A range of evidence can be used to inform reconstructions of river width, including deposit lateral extent (e.g., Wood et al., 2022), numerous depth-scaling relations (e.g., Long, 2021), and barform accretion length (Greenberg *et al.*, 2021). Uncertainty in river width estimates is especially high when considering multi-threaded rivers. Therefore, estimates of width must be made in parallel with planform reconstructions to faithfully reconstruct ancient river morphology. Given previous work which interprets Montllobat and Castissent rivers as multi-threaded (Nijman & Nio, 1975; Van der Meulen, 1989), and results

described below which support this, we used a formula for low-sinuosity rivers based on analysis by Long (2021) which relates bankfull width (W) to bankfull flow depth by:

$$W = 30.296H^{1.211}, \quad (8)$$

in a regression with an R^2 value of 0.61 and N = 990. This gives an estimate of the width of an individual channel (i.e. a single thread) based on values of H, and uncertainty is modelled using a rectangular distribution within the interquartile range of H. Rates of bankfull water and sediment discharge per channel, Q_w, (with units m^3/s) can be estimated according to $Q_w = q_w W$, where q_w is the discharge per unit width. To propagate uncertainty in channel width, we used a triangular distribution within the interquartile range, excluding outlying values that may represent river flow at extreme flow stages, which in multi-threaded rivers may alter active flow width significantly.

Planform

For total water and sediment discharge rates for the full river system, $Q_{s,w(total)}$, the number of threads in an ancient system must be estimated according to $Q_{total} = N_t Q$, where N_t is the average number of active river threads or channels. We used two approaches to reconstruct the planform morphology of the Montllobat and Castissent rivers, described below.

Our first approach is based on dune-bar angular difference, Δ_{db}. The dominant bar mode in rivers is characteristic of planform morphology: lateral and upstream barform accretion is observed mainly in sinuous rivers, with single-threaded and meandering planform (e.g., Miall, 1994; Rowley *et al.*, 2021). A dominantly downstream accreting bar mode is characteristic of low-sinuosity and braided rivers. In stratigraphy, dominant bar mode can be determined by calculating the angular difference between barform accretion orientation and the cross-set palaeoflow direction of dunes migrating atop or around those bars. Where Δ_{db} averages less than 35°, the dominant bar mode is downstream accretion; where $35° \leq \Delta_{db} \geq 135°$, the dominant bar mode is lateral accretion; and where $\Delta_{db} > 135°$, the dominant bar mode is upstream accretion. We are able to cross-check these results using dune cross-set palaeoflow circular variance, after Selley (1968), Le Roux (1992) and Galeazzi *et al.* (2021), explained further in the Supplemental Material.

Our second approach is based on work by Parker (1976) and Lyster et al. (2022). Parker (1976) theoretically derived planform stability fields, expressed as:

$$\varepsilon = \frac{S}{Fr}\frac{H}{W}\ , \tag{9}$$

where $\varepsilon < 1$ for single-threaded rivers, $\varepsilon > 1$ for multi-threaded rivers with 1–10 active channels, $\varepsilon > 10$ for multi-threaded rivers with more than 10 active channels, and Fr is the Froude number, calculated as

$$Fr = \frac{U}{\sqrt{gH}}\ . \tag{10}$$

Lyster et al. (2022a) compiled a dataset of hydraulic geometries in natural rivers, and used these to update the stability fields for river planform geometries based on a much larger observational dataset. We estimate S, Fr, H and W for the rivers of the Montanyana Group and propagate uncertainty to generate a random distribution of 10^6 points within the range of uncertainty on a graph of S/Fr vs H/W to determine the likely planform morphology based on the stability fields of Lyster *et al.* (2022a).

4 RESULTS

4.1 Palaeohydrology Through Time

Through a comprehensive quantitative suite of palaeohydrologic techniques, we reconstruct the evolving morphodynamics of the Eocene Montllobat and Castissent formations, and the rates and styles of water and sediment flow through these ancient river systems.

Based on full measured cross-set thickness distributions, the mean preserved cross-set thickness, h_{xs}, in the Montllobat fluvial sand bodies is 7.8 cm, and 7.5 cm in the Castissent fluvial deposits. Our dataset describes cross-set thickness across the full down-system transects of c. 13 km in the Montllobat and c. 28 km in the Castissent, and there are no strong down-system trends in h_{xs} or grain-size (Supplemental Material). Therefore, we present results spatially averaged for each interval (the distribution of field data is presented on Figure 1 and Figure 3A). Using Equation 1 (Leclair & Bridge, 2001) we estimate that original dune height, h_d, averages 23 cm in the Montllobat and 22 cm in the Castissent. Two-tailed Kolmogorov-Smirov (K-S) tests unambiguously show that the full distributions of cross-sets from each Formation are statistically different with 98.9% confidence, despite the medians being similar, while each member of the formations has cross-set thickness distributions which are statistically similar within each formation (Fig. 6A, bottom x-axis). This demonstrates that the

Castissent and Montllobat formations do have physically different properties to one-another at bedfom-scale.

The depth-scaling relation of Bradley & Venditti (2017) uses values of h_d to reconstruct median formative flow depths, H, of 1.36 m in the Montllobat Formation and 1.26 m in the Castissent (Eq. 2). Similarly to the original bedform data, the full distributions of reconstructed depths (Fig. 6A, top x-axis) are statistically different between the two formations, suggesting formative flow in the Castissent was marginally shallower. Further constraints were made on flow depth based on a barform approach, using the heights of bar accretion sets, h_{acc}. The median barform-derived flow depth is 1.40 m in both the Montllobat and the Castissent formations, with mean values of 1.42 m and 1.85 m, respectively. These results indicate that bedform- and barform-derived flow depth reconstructions are concurrent, and confirm that assumptions of barform and bedform preservation inherent to the methods used are appropriate for these units.

Fluvial channels in the Montllobat Formation are dominated by medium-grained sandstone, with an overall D_{50} of 0.38 mm. Castissent rivers had a bedload of coarse sand averaging 0.94 mm, however, both units contain some channelised, gravel-dominated conglomerates. Using estimates of H and D_{50}, we used Equation 3 (Trampush et al., 2014) to reconstruct channel palaeoslope, S. We find that Montllobat rivers had a median slope of 8.0×10^{-4} m/m (or 0.8 m/km) and Castissent rivers were 40% steeper with a median S value of 1.2×10^{-3} m/m. K-S tests on the full distribution of slope values (Fig. 6B), after Monte Carlo uncertainty propagation, demonstrate this increase in slope during the Castissent interval is statistically significant to 100.0% confidence.

These results show a clear change in palaeohydrological conditions between the two formations, but analysis at member level permits further temporal granularity in our analysis. Figure 7 illustrates changing H and S through the Montllobat and Castissent formations at member-level, between 53.0 and 49.7 Ma. This reveals a steady shallowing in flow depth through time, coupled with a sharp increase in palaeoslope at the start of the Castissent interval, peaking in Castissent B.

Palaeohydraulic calculations also show that the unit water discharge and unit sediment discharge increase in the Castissent interval. Reconstructed H and S give median flow velocity, U, as 1.16 m/s in the Montllobat and 1.29 m/s in the Castissent (Eq. 4). We then reconstruct q_w

which averages 1.57 m^2/s in the Montllobat, and increases to 1.66 m^2/s by c. 50 Ma (Fig. 8A, Eq. 5). Our sediment transport approach yields median unit sediment flux rates, q_s, of $3.6x10^{-3}$ m^2/s in the Montllobat and $2.6x10^{-3}$ m^2/s in the Castissent (Fig. 8B). Normalised per unit width and averaged per formation, water flux increases across the base of the Castissent, and sediment flux decreases. However, member-level palaeohydrologic reconstructions (Figure 8B) reveal a consistent increase in unit sediment flux through the Castissent Formation. Median formation-level unit water and sediment fluxes are skewed down by Castissent A which contains the majority of cross-set data, and is consistently most similar hydrologically to the Montllobat Formation. Note that these estimates do not consider the widths of river channel threads or of the total river channel belt.

4.2 Planform and Palaeoflow

Using palaeohydrological field observations, we use two quantitative approaches to reconstruct the palaeo-planforms of the rivers of the Montllobat and Castissent formations through time. Our first approach to reconstructing fluvial planform morphology is a dune-bar angular difference approach rooted in primary observational data. The median difference in orientation between preserved dune cross-set lee faces and barform accretion surfaces, Δ_{db}, in the Montllobat Formation is 54°, 53° in MlbA and 59° in MlbB. In the Castissent Formation, the median Δ_{db} value is 38°, and in CstA, CstB and CstC the median Δ_{db} is 40°, 37° and 25° respectively (Fig. 9A, Table 2). Downstream, lateral and upstream accreting bars are noted in multiple fluvial styles, but where a fluvial deposit dominantly preserves a certain bar mode, they can be used to interpret palaeo-planform. As the angular difference between the cross-set lee faces and barform accretion surface orientation decreases, bars increasingly represent downstream accretion, characteristic of multichannel braided systems. As illustrated in Figure 9A, this method of extracting bar modes from fluvial stratigraphy reveals a transition from more lateral-accretion-dominated planforms into a predominantly downstream-accretion-dominated planform over time, suggesting rivers became more braided in the Castissent interval. This is supported by low observed cross-set palaeoflow circular variance values, which are between 0.11 and 0.31 for the Montllobat (IQR) and 0.14 – 0.48 for the Castissent, with values as low as 0.04. This signature of low-variance dune migration is consistent with low-sinuosity multi-threaded river systems (Galeazzi *et al.*, 2021).

Our second approach, based on planform stability, ε (Parker, 1976; Lyster *et al.*, 2022a), requires estimates of river width. Using Equation 8, we calculate channel width, W, from both

barform and bedform approaches to reconstructing flow depth, which give similar results (Fig. 10). Using bedform-derived H estimates, individual river channels in the Montllobat Formation had median widths of 44 m, and using barform-derived H values, channels averaged 45 m wide. For the Castissent Formation, the median bedform-derived W estimate is 40 m, and using the barform approach, channels could have been 46 m wide. In further analysis, we favour the barform-derived estimates of channel width, as they represent more robust architectural constraints on channel morphology and introduce fewer uncertainties.

We model the number of active channel threads, N_t, using a rectangular distribution of values within the range of uncertainty. To estimate a maximum N_t, we used the average width of amalgamated multilateral sandstone bodies observed. In the Castissent Formation, sandstone bodies average 1.0 km wide, and the average is 0.5-0.6 km in the Montllobat Formation. These represent conservative lower limits on the width of the alluvial plain, and an upper limit on the width of active flow. Therefore, we use these values along with estimates of W, above, to calculate the likely maximum number of channel threads by dividing estimated channel width and proportion into the estimated alluvial plain width for each formation. This is $N_t = 7$ in the Montllobat and $N_t = 11$ in the Castissent. We set the lower limit for N_t as 1 in the Montllobat and 2 in the Castissent, given we and others (Cabello *et al.*, 2018) identify single-threaded reaches in the Montllobat, but interpret the Castissent as braided, with no single-threaded reaches (see Supplemental Materials for full uncertainty distributions). These yield median total active flow widths, W_{total}, of 205 and 225 m in the Montllobat and Castissent Formations, respectively. Using estimates of W_{total}, Fr, H and U (Eq. 10), planform geometry can be compared to stability fields generated based on theory and observations of modern and ancient rivers (Parker, 1976; Lyster *et al.*, 2022a). Figure 9B shows that according to the dataset of Lyster (2022), the typical median Castissent river was stable in a braided planform. This approach suggests Montllobat rivers had some single-threaded reaches but were broadly stable with an anastomosing planform, defined by Lyster (2022) as $S/Fr > 0.003$ and $H/W < 0.2$. Makaske (2001) defines anastomosing rivers as composed of two or more interconnected channels that enclose floodbasins. This interpretation is supported by facies observations, including those of Cabello *et al.* (2018).

To summarise, recovered bar modes and planform stability analysis shows that what started as anastomosing rivers with some single-threaded reaches transitioned into braided systems by the time of the Castissent interval.

4.3 Total Water and Sediment Fluxes

The above palaeohydraulic reconstructions of unit discharges and unit sediment fluxes explicitly do not include channel width, which is the most challenging aspect of this type of stratigraphic reconstruction (Long, 2021). However, combining unit fluxes with river planform estimates and thread width estimates (Figures 9 and 10), we can investigate foreland-scale geomorphology in the early Pyrenees by estimating total water and sediment loads to first order, as represented in the Montanyana Group.

Total active flow widths are estimated to average 205 and 225 m respectively for the Montllobat and Castissent Formations. Since total discharge is a product of unit discharge and total active flow width, we use our results to reconstruct a median estimate of $Q_{w(total)}$ in the Montllobat Formation of ca. 280 m^3/s, and ca. 420 m^3/s in the Castissent, a 40% increase. For total sediment discharge, $Q_{s(total)}$ increased from 0.6 m^3/s in the Montllobat to 0.7 m^3/s in the Castissent, a 10-15% difference at median level. Whilst this change in sediment flux appears modest, Figure 11 depicts graphically the changing total fluxes and uncertainty, and highlights a consistent increase in sediment load through time. These estimates quantitatively describe material flux through the rivers of the Eocene Hothouse, and how they behaved in space and time. We now consider these deposits in the context of regional climate and tectonics in the lower Eocene, and compare reconstructed fluvial hydrology to modern and ancient rivers, posing the question: what caused the hydrological change interpreted at the base of the Castissent Formation?

5 DISCUSSION

5.1 Modern Comparisons

Using a suite of quantitative palaeohydrologic techniques based on geologic field data, we reveal the lower Eocene rivers of the Montanyana Group became increasingly multi-threaded through time, and were on average 1.2 – 1.4 m deep (but could be deeper than 5 m, based on maximum barform accretion set thicknesses), with channel slopes of 0.5 – 0.7°. We reconstruct a marked increase in river slope and discharge at 50.5 Ma, and a shift in planform coinciding with the onset of Castissent progradation and an increase in water and sediment discharge, supporting and furthering the findings of previous facies-architectural and stratigraphic investigations. This represents the most robust quantitative description of Ypresian rivers in the Pyrenees to date, summarised in Figure 12. How comparable are these rivers to modern

examples, given they were deposited during a period of marked global warmth compared to today?

We compare results to a global database of modern river morphology and hydrology (Lyster *et al.*, 2022a), and find that there are no identical modern analogues for the Montllobat and Castissent systems. This is consistent with expectations of fluvial systems active in a unique tectono-climatic setting in the south Pyrenean Foreland during the EECO, the likes of which do not exist on Earth today. Solely considering similarity in planform, discharge, width, slope and grain-size, they were superficially similar to the Tanana and Saskatchewan rivers, Alaska; Athabasca river, Canada; Wairau river, New Zealand; Durack river, northwestern Australia; or the Yuma Wash river, Arizona. However, on average, reconstructed *W/H* ratios were lower in the Montanyana Group than in most modern sand-bedded multi-threaded rivers with similar water discharge rates. Moreover, modern multi-threaded sand-bedded rivers have flow velocity averaging 1.0 m/s, slower than those in the lower Eocene Pyrenean foreland. This suggests either a bias in our results related to the preservation potential of small rivers, or suggesting Montanyana rivers were somewhat deeper and faster than modern analogues with similar planform.

Furthermore, geochemical data acquired from Castissent floodplain deposits show the environment of the early Eocene was semi-arid to sub-humid with seasonal humidity patterns (Honegger *et al.*, 2020). Today, few braided, sand-bed rivers with similar water discharge rates are observed in regions with seasonally subhumid climate (Beck *et al.*, 2018). Considering these constraints, the closest modern analogues for the Castissent Formation are the braided Gangetic rivers of the Himalayan foreland, with comparable fluvial morphology, climate characteristics and tectonic setting to that in the lower Eocene, albeit with much larger catchments and discharge rates (Lyster *et al.*, 2022a). The Montanyana rivers' flow velocity, aspect ratio, planform and bedload grain-size, all in a small orogenic setting and sub-arid climate make this Eocene system unique compared to rivers today. What antecedent conditions permitted this, and what caused the changes in hydrology we reconstruct?

5.2 Climate and Tectonics in the Eocene Pyrenees

Disentangling the competing signals of climatic and tectonics in the fluvial archive is an ongoing research challenge. The Montanyana Group was deposited within a foreland basin setting of a growing mountain belt, at a time of exceptional climate warmth compared to today,

546 so we might expect to see the impact of both these drivers expressed in the stratigraphic archive.
547 Our results, for instance, show a clear climate signature recorded in fluvial channel sediment:
548 The Castissent rivers had 40% more water discharge yet only 10-15% greater sediment
549 discharge, and were more strongly braided in comparison to the underlying Montllobat
550 Formation. Notably, the ratio of Q_s to Q_w (the sediment flux intensity) is nearly 50% lower in
551 the Castissent, meaning it transported more water per unit sediment discharge than the
552 Montllobat. These changes point to a climatic driver, because they imply a change to the
553 frequency/magnitude distributions of water discharge. We also reconstruct a 1.4-fold increase
554 in channel slope. A slope increase could be driven by a reduction in precipitation (c.f. D'Arcy
555 & Whittaker, 2014), but given increasing water discharge we hypothesise steepening was
556 forced by tectonics. Consequently, we first discuss what tectonic drivers may have affected
557 sedimentation in the Tremp-Graus Basin and how we can we isolate them, before exploring
558 how climate influenced the Montanyana rivers.

559 *Uplift and Exhumation*

560 The sediments of the Montanyana Group were deposited during the dynamic early stages of
561 mountain growth associated with the collision of Iberia and Eurasia. Thermochronologic
562 analyses focused on resolving Pyrenean orogenic history (Whitchurch *et al.*, 2011) suggests
563 there was an increase in tectonically driven bedrock exhumation and a decrease in depositional
564 lag times across the southern Pyrenees focused at c. 50.9 Ma. This is supported by Curry et
565 al.'s (2021) findings that suggest a 2.4-fold increase in exhumation rate in the Castissent's likely
566 headwater region (Fig. 2B) could have contributed to the strong progradation of the Castissent
567 Formation c. 50 Ma.

568 Progradation is well-documented in the Castissent in a stratigraphic context (e.g. Marzo et al.,
569 1988) and is associated with an increase in slope and D_{50} from the Montllobat into the
570 Castissent (averaged across the total dip-section) based on our interpretations, demonstrating a
571 down-system shift in fluvial facies. It has been hypothesised that Castissent progradation could
572 be related to an Ypresian sea-level fall, reducing accommodation space and increasing
573 amalgamation of fluvial sand bodies (Marzo *et al.*, 1988; Whitchurch *et al.*, 2011; Honegger *et*
574 *al.*, 2020). However, the Castissent Formation shows a significant increase in stratigraphic
575 thickness westwards (basinwards), which is inconsistent with the basinward reduction in
576 accommodation that is typically expected during progradation forced by sea-level fall (Plint &
577 Nummedal, 2000).

Changing exhumation rates can result in dramatically different fluvial processes and geomorphology, including changing grain-size, slope and down-system facies distribution. The observed increase in slope could therefore have been driven primarily by a change in tectonic uplift rates. A 2.4-fold increase in uplift rate would be sufficient to outpace the climate-driven lowering effects of the reconstructed c. 40% increase in precipitation. However, it is challenging to separate signals of tectonically-driven uplift and exhumation versus climate-driven erosion and denudation using thermochronological techniques. Further spatio-temporal constraints on the thermochronological history of the Castissent's headwater region would permit these interpretations to made with more certainty at a catchment-scale, but we can also approach this problem from a different angle: by investigating climate signals in further detail, using our palaeohydraulic results.

Climate signals

The sediment flux intensity in the Castissent is 46% lower than in the Montllobat, meaning river water carried half as much sediment on average. Not only this, but we reconstruct an absolute increase in Q_w of 40% and Q_s of 15% into the Castissent Formation. To increase Q_w, the simplest and most likely cause is a change in the bankfull-recurrence precipitation rate. Yet, if this discharge is distributed across the annual or long-term hydrograph where thresholds for significant sediment transport are surpassed infrequently, for example in a system characterised by sustained or perennial water discharge, we might expect this change in Q_w to be coupled with a relatively modest change in Q_s,. So we interpret these observations to indicate a change in the magnitude or frequency of rainfall, likely driven by climate change. We observe these effects today (e.g., Beniston *et al.*, 2007; Westra *et al.*, 2014; Piras *et al.*, 2016; Tramblay & Somot, 2018; Hansford *et al.*, 2020; Liu *et al.*, 2021; IPCC, 2022; McLeod *et al.*, 2024), and there are a growing number of stratigraphic case studies documenting the effects of climate change on geomorphic systems, specifically where changing material flux is observed.

As a regional example that has already been well-documented, the Palaeocene-Eocene Thermal Maximum (PETM) is recorded in fluvial successions of the southern Pyrenean Claret Conglomerate (Prieur *et al.*, 2025). Here, a 3-8°C increase in mean annual temperature (MAT) and a 27% increase in mean annual precipitation (MAP) is interpreted to have caused a two-fold increase in Q_s, in addition to heightened rates of channel amalgamation. Additionally, the upper Eocene Escanilla Formation (south Pyrenean Foreland) spanning the Mid Eocene Climate Optimum (MECO) records Q_s increasing rapidly 1.5-fold in intervals with highly

amalgamated sandbodies, compared to low-amalgamation intervals (Sharma *et al.*, 2023). This is interpreted to have been caused by climate-driven water discharge variation, with reductions in slope and 3-fold increases in Q_w. Hyperthermal climate change has also been identified in Ypresian river deposits in the northern Pyrenean basins of France (Boyrie *et al.*, 2025). In this setting, monsoon-type events triggered by transient warming are shown to have increased sediment flux in rivers. Sediment transport is also projected to increase in modern river systems due to current global warming (McLeod *et al.*, 2024).

So changing sediment flux is a documented result of climate change in geomorphic systems in the past and present. It is often associated with increased amalgamation of channel-fill sandstone and conglomerate bodies, but evidently competing climate and tectonic forcings can have varied impacts on geomorphology from source to sink – such as the slope reduction observed in high-discharge intervals of the Escanilla Formation (Sharma *et al.*, 2023), in comparison to the slope increase in the Castissent. This difference likely arose due to the marked increase in exhumation rate in the Castissent catchment attributed to tectonic uplift, which caused steepening to outpace the lowering effects of climate change such as are documented by Sharma *et al.* (2023). The Escanilla outcrop at Olson, Spain, studied by Sharma *et al.* (2023), represents a more distal fluvial setting than the Castissent, so we might not expect significant effects from mountain uplift.

However, despite a clear reconstructed hydrologic shift at the onset of the Castissent Formation, this interval (50.5 – 49.7 Ma) is not associated with a discrete climate signal lasting 0.8 Myrs. On the contrary, the climate during Castissent deposition is characterised by a gradual reduction in global temperatures at the end of the EECO (Fig. 2) and superimposed hyperthermal events. Furthermore, the switch to a heightened uplift rate modelled by Curry et al. (2021, Fig. 2) occurs at 50 Ma, after which high uplift rates are maintained for a prolonged period. A permanent change in tectonic uplift rates should in theory lead to a permanent increase in sediment flux as topographic steady state is re-achieved (Armitage *et al.*, 2011). Conversely, the Castissent Formation represents a discrete 800 kyr period of heightened water and sediment flux, followed by the Upper Montanyana Group and a return to a similar depositional character and facies distribution (Fig. 3) to that of the underlying Montllobat Formation (Nijman & Nio, 1975; Marzo *et al.*, 1988; Nijman, 1998), all whilst high uplift rates continue. The stratigraphic architecture and facies distributions of the Montanyana Group (Fig. 3) imply a geomorphic change that was transient (Nijman, 1998; Armitage *et al.*, 2011), unlike

642 the regional tectonic trends. Consequently, we argue that climate change must play an
643 important role in controlling the timing of geomorphic change in the early Pyrenees.

644 Given examples above of hothouse climates and hyperthermals affecting sedimentology and
645 hydrology in Pyrenean basins, how can these climate signals superimpose with tectonic trends
646 to generate the discrete and transient progradation and hydrological change observed in
647 stratigraphy?

648 *Eocene climate*

649 After the PETM, the Ypresian climate is characterised by a broad warming trend climaxing in
650 the EECO, before a gradual cooling and levelling off by 50 Ma (Fig. 2, Westerhold et al., 2018).
651 Honegger et al. (2020) interpret semi-arid to sub-humid average climates in the Castissent
652 interval based on CaO/Al_2O_3 ratios in floodplain sediment, and seasonal humidity patterns
653 based on the smectite/kaolinite ratio in palaeosols and the presence of nodules composed of
654 concentric haematite and goethite found together with carbonate nodules. In the Montllobat
655 Formation on the other hand, humidity and precipitation rates are not as well-constrained, so
656 interpretations of humidity change at the onset of the Castissent are more speculatory. However,
657 river channel deposits of Montllobat-equivalent age in the northern Pyrenean Minervois Basin
658 interpreted as ephemeral (Boyrie *et al.*, 2025) suggest the climate was also semi-arid to sub-
659 humid, but likely more arid than that of the Castissent.

660 The interval of Castissent deposition contains three hyperthermals recognised in $\delta^{13}C$ records
661 of benthic carbonates (Westerhold *et al.*, 2017; Honegger *et al.*, 2020). Hyperthemal "S"
662 coincides with the onset of Castissent sedimentation, followed shortly by hyperthermal "T,"
663 but Honegger et al. (2020) identify only the geochemical signature of the subsequent
664 hyperthermal "U" recorded in the floodplain above Castissent A in the Chiriveta section (Fig.
665 1, 2). It is dated to 50.0 Ma and is associated with a MAT increase of 2 - 3°C that could have
666 had a duration as short as 40 kyrs, but preserves a signal climax lasting 150 kyrs (c. 50.10 –
667 49.95 Ma) in stratigraphy – the duration likely augmented by the dynamic nature of fluvial
668 deposition (Honegger *et al.*, 2020). Significantly, we do not see a uniform signal across the
669 Castissent Formation, but Castissent B which was likely deposited during c. 50.0 – 49.8 Ma
670 preserves the most significant signal of enhanced S and Q_w, followed by Q_s peaking in
671 Castissent C (Fig. 8). Therefore, the onset of the Castissent could be related to hyperthermals
672 "S" and "T" (Fig. 2A). Subsequently, the prolonged signal of hyperthermal "U", representing

673 the delayed fluvial response to a negative $\delta^{13}C$ excursion, could be manifest in the rock record
674 in the geomorphology of Castissent B followed by an enhancement in sediment flux in
675 Castissent C potentially driven by a disequilibrium channel slope change controlled by tectonic
676 uplift.

677 The strong change in formative discharge conditions observed at both channel and braidplain
678 scale in the absence of large changes in yearly rainfall typically relates to the distribution and
679 magnitude of individual storm or monsoon events (Molnar *et al.*, 2006). Specifically, the
680 reconstructed 46% reduction in sediment flux intensity coupled with absolute increases in both
681 Q_s and Q_w at the base of the Castissent points to more sustained precipitation which leads to
682 sediment transport sediment as a lower proportion of the water discharge. What could have
683 caused these changes to river hydrographs in the lower Eocene?

684 Palaeobotanial proxies (Greenwood & Huber, 2011) suggest that throughout the early-mid
685 Eocene, Earth's climate was controlled by a global monsoon cycle, driving strongly seasonal
686 precipitation patterns. It has also been observed that temperature increase causes enhanced
687 monsoon cycles (Loo *et al.*, 2015), and interpreted that warming caused increased humidity
688 and precipitation in the PETM of the Pyrenees (Prieur *et al.*, 2025). We now investigate
689 whether palaeohydrology support this hypothesis, and if the three global CIE hyperthermals
690 between 50.5 and 49.7 Ma could have affected monsoon cycles to cause the stratigraphic
691 marker of the Castissent Formation.

692 Hydrological calculations suggest discharge in the Montanyana rivers was variable enough to
693 imply monsoonal rainfall patterns: if we model the MAP of 376 mm/a (Honegger *et al.*, 2020)
694 to rain on an estimated Castissent catchment of c. 10,000 km^2 – based on compiled
695 palaeogeographic reconstructions and independent constraints on altimetry and sediment
696 routing (Huyghe *et al.*, 2012; Curry *et al.*, 2019; Markwick, 2019; Juvany *et al.*, 2024) – this
697 implies mean flow of under 1/3 the discharge of channel-forming conditions reconstructed
698 here. From this we could estimate a monsoon precipitation index (MPI, Wang & Ding, 2008),
699 i.e., the ratio between the annual precipitation range and the MAP. We assume here this is
700 equivalent to the difference between the bankfull and mean annual discharge (MAD), divided
701 by the MAD. This calculation yields a value of 2.5, suggesting strongly variable rainfall that
702 could have been driven by the monsoon cycles documented by Greenwood & Huber (2011).
703 This supports the geochemical findings of Honegger et al. (2020) that the climate was highly

seasonal, and the findings of Boyrie *et al.* (2025) for Ypresian river systems in the northern Pyrenees.

Plink-Bjorklund (2015) compiled a series of facies indicators for monsoon-dominated fluvial systems in the rock record: these types of rivers are often dominated by downstream accreting bars and an absence of well-preserved lateral accretion, and these indicators are increasingly dominant up-section (Fig. 9A). However, monsoonal systems characterised by ephemeral transport are also expected to record dominant soft sediment deformation, fossilised in-channel vegetation and upper-flow regime sedimentary structures (Plink-Bjorklund, 2015). We observe these rarely in the Montanyana Group, implying a strengthening monsoon in an increasingly humid environment.

Considering the reconstructed palaeohydrology, in addition to constraints on climate and tectonics from thermochronology and sedimentary geochemistry, we hypothesise that the levelling-off in global cooling at the end of the EECO followed by three hyperthermal events may have driven changes to the global monsoon cycle, increasing the frequency of precipitation in the Pyrenees. This in turn cause water and sediment discharge in the Montanyana rivers to increase. There is strong precedent for climate-driven change to monsoon cycles on similar timescales in the active tectonic setting of the Himalaya. Modern climate change and tectonic uplift of the Himalayan plateau has enhanced monsoon cycles, altering river hydrology in the present-day foreland (Loo *et al.*, 2015). Similar effects are reconstructed in the same setting 4.2 ka when abrupt cooling caused monsoon cycles to weaken, significantly reducing Indus river discharge, affecting communities as a consequence (Giosan *et al.*, 2012; Dixit *et al.*, 2014; Dutt *et al.*, 2018). So it seems reasonable that high-frequency climate change could have caused a shift in monsoon discharge and river activity in the Montanyana rivers. Perhaps the modern Himalaya are a strong analogue for the evolving Montanyana rivers – with a similar tectono-climatic setting and with abrupt increases in temperature and humidity strengthening monsoon cycles and affecting hydrology.

Comparing the global $\delta^{13}C$ record with exhumation profiles for the Ypresian Pyrenees (Fig. 2) establishes that the observed morphological and hydrodynamic shift observed at 50.5 Ma occurs at the superimposition of a gradual global cooling, an increase in hinterland exhumation rate, and the occurrence of three transient hyperthermal events. We hypothesise that during early mountain growth and in a gradually cooling climate from 53 – 50.5 Ma, the Montllobat rivers adopted stable multithreaded (anastomosing) planform and transported a bedload of

736 medium sand as a large proportion of its water discharge, consistent with observed Q_s/Q_w ratios.
737 The overlying Castissent then saw the cooling trend level off, and a briefly enhanced global
738 monsoon driven by three successive hyperthermal events. Simultaneously, an increase in
739 Pyrenean tectonic uplift forced a steepening of the catchment. Triggered by this, rivers became
740 temporarily faster and more strongly braided, with more sustained water discharge and
741 transport of coarse sediment from the growing Pyrenees lasting 800 kyrs, resulting in a 20 km
742 progradation of fluvial facies.

743 In this palaeohydrological analysis, we have identified and quantitatively described a
744 significant geomorphic change 50 Mya, and isolated the specific climatic and tectonic drivers
745 that affected rivers and landscapes in this dynamic hothouse environment. The remaining
746 unknowns concern the potential role of the patterns of climate-driven precipitation in driving
747 fluvial geomorphic change in the Montanyana Group, specifically channel slope, and the
748 detailed palaeohydrology of the Upper Montantyana Group. In order to comprehensively
749 disentangle climate change from the tectonic signal of the growing Pyrenees, mean conditions
750 are not enough. The frequency and patterns of threshold-surpassing events – river intermittency
751 – could be what controls transient landscape response to climate drivers (McLeod *et al.*, 2024).
752 Combined with this study's quantification of landscape-scale fluvial geomorphology, this next
753 step could complete the picture of landscape dynamics in the Montanyana Group.

754 **6 CONCLUSION**

755 The lower Eocene Montllobat and Castissent formations of the southern Pyrenees record a
756 geomorphic event towards the end of the EECO which saw coarse-grained fluvial sandstones
757 prograde 20 km seaward within an 800 ka period. Using a quantitative field-based
758 palaeohydrologic framework across 4 field sites, we establish strong constraints on the
759 evolving hydrodynamics of these ancient river systems. We show that the start of the Castissent
760 interval at c. 50.5 Ma is associated with a statistically significant reduction in cross-set
761 thickness, a doubling of the median grain-size and a 1.4-fold increase in channel slope. We
762 reconstruct a 40% increase in total water discharge from the Montllobat to the Castissent
763 Formation, a 15% increase in sediment discharge, and a signature of sustained precipitation.
764 We also quantify a shift in fluvial planform morphology: Castissent rivers exhibited more
765 pronounced braiding than the mostly anastomosing Montllobat Formation before it, and we
766 track these trends through time, showing a sharp change in hydrodynamics at the base of the
767 Castissent Formation. These results, in combination with climate and exhumation records for

the southern Pyrenees, suggest that the Castissent Formation represents the transient product of multiple climatic signals within the context of an evolving mountain range: a levelling off in a long-term cooling trend at the end of the EECO, three superimposed hyperthermal events, and an increase in tectonic uplift rate at c. 50.5 Mya. We hypothesise this climate change caused enhanced monsoon precipitation and more sustained river discharge, driving a significant shift in fluvial hydrodynamics and geomorphology. This analysis sheds light on river dynamics in an environment analogous to a future climate scenario, and reveals the potential in quantitative palaeohydrology to extract complex tectono-climatic signals from stratigraphy. Further investigation into the patterns of water and sediment transport through the lower Eocene could help determine the extent to which climate change can cause significant shifts in fluvial activity and landscape dynamics.

BIBLIOGRAPHY

Allen, P.A. (2008) From landscapes into geological history. *Nature*, **451**, 274–276.

Allmendinger, R.W., **C., C., N.** and **Fisher, D.** (2013) Structural Geology Algorithms: Vectors & Tensors.

Armitage, J.J., **Duller, R.A.**, **Whittaker, A.C.** and **Allen, P.A.** (2011) Transformation of tectonic and climatic signals from source to sedimentary archive. *Nature Geosci*, **4**, 231–235.

Beck, H.E., **Zimmermann, N.E.**, **McVicar, T.R.**, **Vergopolan, N.**, **Berg, A.** and **Wood, E.F.** (2018) Present and future Köppen-Geiger climate classification maps at 1-km resolution. *Sci Data*, **5**, 180214.

Beniston, M., **Stephenson, D.B.**, **Christensen, O.B.**, **Ferro, C.A.T.**, **Frei, C.**, **Goyette, S.**, **Halsnaes, K.**, **Holt, T.**, **Jylhä, K.**, **Koffi, B.**, **Palutikof, J.**, **Schöll, R.**, **Semmler, T.** and **Woth, K.** (2007) Future extreme events in European climate: an exploration of regional climate model projections. *Climatic Change*, **81**, 71–95.

Boyrie, C., **Girard, F.**, **Yans, J.**, **Ballas, G.**, **Lihoreau, F.**, **Benammi, M.**, **Bourget, H.**, **Garcia, G.**, **Leredde, C.**, **Pellissier-tanon, A.**, **Valentin, X.**, **Vidalenc, D.** and **Tabuce, R.** (2025) Abrupt changes in continental sedimentation triggered by monsoon-type event during EECO hyperthermals, Minervois Basin, Southern France. *Sedimentary Geology*, 106923.

Bradley, R.W. and **Venditti, J.G.** (2017) Reevaluating dune scaling relations. *Earth-Science Reviews*, **165**, 356–376.

Broz, A.P., **Pritchard-Peterson, D.**, **Spinola, D.**, **Schneider, S.**, **Retallack, G.** and **Silva, L.C.R.** (2024) Eocene (50–55 Ma) greenhouse climate recorded in nonmarine rocks of San Diego, CA, USA. *Sci Rep*, **14**, 2613.

Cabello, P., **Domínguez, D.**, **Murillo-López, M.H.**, **López-Blanco, M.**, **García-Sellés, D.**, **Cuevas, J.L.**, **Marzo, M.** and **Arbués, P.** (2018) From conventional outcrop datasets and digital outcrop models to flow simulation in the Pont de Montanyana point-bar deposits (Ypresian, Southern Pyrenees). *Marine and Petroleum Geology*, **94**, 19–42.

Caja, M.A., **Marfil, R.**, **Garcia, D.**, **Remacha, E.**, **Morad, S.**, **Mansurbeg, H.**, **Amorosi, A.**, **Martínez-Calvo, C.** and **Lahoz-Beltrá, R.** (2010) Provenance of siliciclastic and hybrid turbiditic arenites of the Eocene Hecho Group, Spanish Pyrenees: implications for the tectonic evolution of a foreland basin. *Basin Research*, **22**, 157–180.

Castelltort, S. and **Van Den Driessche, J.** (2003) How plausible are high-frequency sediment supply-driven cycles in the stratigraphic record? *Sedimentary Geology*, **157**, 3–13.

Chamberlin, E.P. and **Hajek, E.A.** (2019) Using bar preservation to constrain reworking in channel-dominated fluvial stratigraphy. *Geology*, **47**, 531–534.

Chanvry, E., **Deschamps, R.**, **Joseph, P.**, **Puigdefàbregas, C.**, **Poyatos-Moré, M.**, **Serra-Kiel, J.**, **Garcia, D.** and **Teinturier, S.** (2018) The influence of intrabasinal tectonics in the stratigraphic evolution of piggyback basin fills: Towards a model from the Tremp-Graus-Ainsa Basin (South-Pyrenean Zone, Spain). *Sedimentary Geology*, **377**, 34–62.

Clark, J.D. and **Pickering, K.T.** (1996) Architectural Elements and Growth Patterns of Submarine Channels: Application to Hydrocarbon Exploration1. *AAPG Bulletin*, **80**, 194–220.

Colombera, L., **Arévalo, O.J.** and **Mountney, N.P.** (2017) Fluvial-system response to climate change: The Paleocene-Eocene Tremp Group, Pyrenees, Spain. *Global and Planetary Change*, **157**, 1–17.

Cornard, P. and **Pickering, K.** (2020) Submarine topographic control on distribution of supercritical-flow deposits in lobe and related environments, middle Eocene, Jaca Basin, Spanish Pyrenees. *Journal Of Sedimentary Research*, 1222–1243.

Curry, M.E., **Beek, P.V.D.**, **Huismans, R.S.**, **Wolf, S.G.**, **Fillon, C.** and **Muñoz, J.-A.** (2021) Spatio-temporal patterns of Pyrenean exhumation revealed by inverse thermo-kinematic modeling of a large thermochronologic data set. *Geology*, **49**, 738–742.

Curry, M.E., **van der Beek, P.**, **Huismans, R.S.**, **Wolf, S.G.** and **Muñoz, J.-A.** (2019) Evolving paleotopography and lithospheric flexure of the Pyrenean Orogen from 3D flexural modeling and basin analysis. *Earth and Planetary Science Letters*, **515**, 26–37.

D'Arcy, M. and **Whittaker, A.C.** (2014) Geomorphic constraints on landscape sensitivity to climate in tectonically active areas. *Geomorphology*, **204**, 366–381.

Das, D., **Ganti, V.**, **Bradley, R.**, **Venditti, J.**, **Reesink, A.** and **Parsons, D.R.** (2022) The Influence of Transport Stage on Preserved Fluvial Cross Strata. *Geophysical Research Letters*, **49**, e2022GL099808.

Dixit, Y., **Hodell, D.A.** and **Petrie, C.A.** (2014) Abrupt weakening of the summer monsoon in northwest India ~4100 yr ago. *Geology*, **42**, 339–342.

Dutt, S., **Gupta, A.K.**, **Wünnemann, B.** and **Yan, D.** (2018) A long arid interlude in the Indian summer monsoon during ~4,350 to 3,450 cal. yr BP contemporaneous to displacement of the Indus valley civilization. *Quaternary International*, **482**, 83–92.

Emiliano Mutti and **Maria Sgavetti** (1987) Sequence stratigraphy of the upper cretaceous aren strata in the orcau-aren region, south-central pyrenees, spain: distinction between eustatically and tectonically controlled depositional sequences. *Annali Dell'Universita di Ferrara Sezione Scienze Della Terra*, **1**, 1–21.

Engelund, F. and **Hansen, E.** (1967) A monograph on sediment transport in alluvial streams.

Fielding, C.R., **Alexander, J.** and **Allen, J.P.** (2018) The role of discharge variability in the formation and preservation of alluvial sediment bodies. *Sedimentary Geology*, **365**, 1–20.

Fisher, Q.J., **Casey, M.**, **Clennell, M.B.** and **Knipe, R.J.** (1999) Mechanical compaction of deeply buried sandstones of the North Sea. *Marine and Petroleum Geology*, **16**, 605–618.

Flannigan, M.D., **Amiro, B.D.**, **Logan, K.A.**, **Stocks, B.J.** and **Wotton, B.M.** (2006) Forest Fires and Climate Change in the 21ST Century. *Mitig Adapt Strat Glob Change*, **11**, 847–859.

Galeazzi, C.P., **Almeida, R.P.** and **do Prado, A.H.** (2021) Linking rivers to the rock record: Channel patterns and paleocurrent circular variance. *Geology*, **49**, 1402–1407.

Ganti, V., **Whittaker, A.C.**, **Lamb, M.P.** and **Fischer, W.W.** (2019) Low-gradient, single-threaded rivers prior to greening of the continents. *Proceedings of the National Academy of Sciences*, **116**, 11652–11657.

Gariano, S.L. and **Guzzetti, F.** (2016) Landslides in a changing climate. *Earth-Science Reviews*, **162**, 227–252.

Giosan, L., **Clift, P.D.**, **Macklin, M.G.**, **Fuller, D.Q.**, **Constantinescu, S.**, **Durcan, J.A.**, **Stevens, T.**, **Duller, G.A.T.**, **Tabrez, A.R.**, **Gangal, K.**, **Adhikari, R.**, **Alizai, A.**, **Filip, F.**, **VanLaningham, S.** and **Syvitski, J.P.M.** (2012) Fluvial landscapes of the Harappan civilization. *Proceedings of the National Academy of Sciences*, **109**, E1688–E1694.

Greenberg, E., **Ganti, V.** and **Hajek, E.** (2021) Quantifying bankfull flow width using preserved bar clinoforms from fluvial strata. *Geology*, **49**, 1038–1043.

Greenwood, D.R. and **Huber, M.** (2011) Eocene precipitation: a global monsoon? **2011**, T22C-07.

Hansford, M.R., **Plink-Björklund, P.** and **Jones, E.R.** (2020) Global quantitative analyses of river discharge variability and hydrograph shape with respect to climate types. *Earth-Science Reviews*, **200**, 102977.

Honegger, L., **Adatte, T.**, **Spangenberg, J.E.**, **Rugenstein, J.K.C.**, **Poyatos-Moré, M.**, **Puigdefàbregas, C.**, **Chanvry, E.**, **Clark, J.**, **Fildani, A.**, **Verrechia, E.**, **Kouzmanov, K.**, **Harlaux, M.** and **Castelltort, S.** (2020) Alluvial record of an early Eocene hyperthermal within the Castissent Formation, the Pyrenees, Spain. *Clim. Past*, **16**, 227–243.

Huyghe, D., **Mouthereau, F.** and **Emmanuel, L.** (2012) Oxygen isotopes of marine mollusc shells record Eocene elevation change in the Pyrenees. *Earth and Planetary Science Letters*, **345–348**, 131–141.

IPCC (2022) IPCC, 2022: Climate Change 2022: Impacts, Adaptation, and Vulnerability. Contribution of Working Group II to the Sixth Assessment Report of the Intergovernmental Panel on Climate Change. *Cambridge University Press, Cambridge, UK and New York, NY, USA*.

Jaimes-Gutierrez, R., **Adatte, T.**, **Pucéat, E.**, **Vennemann, T.**, **Prieur, M.**, **Wild, A.L.**, **Khozyem, H.**, **Vaucher, R.** and **Castelltort, S.** (2024) Deciphering Paleocene-Eocene Thermal Maximum Climatic Dynamics: Insights From Oxygen and Hydrogen Isotopes in Clay Minerals of Paleosols From the Southern Pyrenees. *Paleoceanography and Paleoclimatology*, **39**, e2024PA004858.

Jerolmack, D.J. and **Paola, C.** (2010) Shredding of environmental signals by sediment transport. Geophysical Research Letters. doi: 10.1029/2010GL044638

Juvany, P., **Garcés, M.**, **López-Blanco, M.**, **Valero, L.**, **Amorós, E.B.**, **Poyatos-Moré, M.** and **Rius, A.M.** (2024) Unraveling the sediment routing systems evolution of the south Pyrenean foreland basin during the lower to middle Paleogene period. *Marine and Petroleum Geology*, **167**, 106913.

Le Roux, J.P. (1992) Determining the channel sinuosity of ancient fluvial systems from paleocurrent data. *Journal of Sedimentary Research*, **62**, 283–291.

Leclair, S. and **Bridge, J.** (2001) Quantitative Interpretation of Sedimentary Structures Formed by River Dunes. *Journal of Sedimentary Research - J SEDIMENT RES*, **71**, 713–716.

Liu, H., **Yi, Y.** and **Jin, Z.** (2021) Sensitivity Analysis of Flash Flood Hazard on Sediment Load Characteristics. *Front. Earth Sci.*, **9**, 683453.

Long, D.G.F. (2021) Trickling down the paleoslope: an empirical approach to paleohydrology. *Earth-Science Reviews*, **220**, 103740.

Loo, Y.Y., **Billa, L.** and **Singh, A.** (2015) Effect of climate change on seasonal monsoon in Asia and its impact on the variability of monsoon rainfall in Southeast Asia. *Geoscience Frontiers*, **6**, 817–823.

Lyster, S.J., **Whittaker, A.C.**, **Allison, P.A.**, **Lunt, D.J.** and **Farnsworth, A.** (2020) Predicting sediment discharges and erosion rates in deep time—examples from the late Cretaceous North American continent. *Basin Research*, **32**, 1547–1573.

Lyster, S.J., **Whittaker, A.C.**, **Farnsworth, A.** and **Hampson, G.J.** (2023) Constraining flow and sediment transport intermittency in the geological past. *GSA Bulletin*, **136**, 2425–2442.

Lyster, S.J., **Whittaker, A.C.** and **Hajek, E.A.** (2022a) The problem of paleo-planforms. *Geology*, **50**, 822–826.

Lyster, S.J., **Whittaker, A.C.**, **Hajek, E.A.** and **Ganti, V.** (2022b) Field evidence for disequilibrium dynamics in preserved fluvial cross-strata: A record of discharge variability or morphodynamic hierarchy? *Earth and Planetary Science Letters*, **579**, 117355.

Lyster, S.J., **Whittaker, A.C.**, **Hampson, G.J.**, **Hajek, E.A.**, **Allison, P.A.** and **Lathrop, B.A.** (2021) Reconstructing the morphologies and hydrodynamics of ancient rivers from source to sink: Cretaceous Western Interior Basin, Utah, USA. *Sedimentology*, **68**, 2854–2886.

Makaske, B. (2001) Anastomosing rivers: a review of their classification, origin and sedimentary products. *Earth-Science Reviews*, **53**, 149–196.

Manning, R., **Griffith, J.P.**, **Pigot, T.F.** and **Vernon-Harcourt, L.F.** (1890) On the flow of water in open channels and pipes. 161 pp.

Markwick, P.J. (2019) Palaeogeography in exploration. *Geol. Mag.*, **156**, 366–407.

Marzo, M., **Nijman, W.** and **Puigdefabregas, C.** (1988) Architecture of the Castissent fluvial sheet sandstones, Eocene, South Pyrenees, Spain. *Sedimentology*, **35**, 719–738.

McInerney, F. and **Wing, S.** (2011) The Paleocene-Eocene Thermal Maximum: A Perturbation of Carbon Cycle, Climate, and Biosphere with Implications for the Future. *Annu. Rev. Earth Planet. Sci.*, **39**, 489–516.

McLeod, J.S., **Whittaker, A.C.**, **Bell, R.E.**, **Hampson, G.J.**, **Watkins, S.E.**, **Brooke, S.A.S.**, **Rezwan, N.**, **Hook, J.**, **Zondervan, J.R.**, **Ganti, V.** and **Lyster, S.J.** (2024) Landscapes on the edge: River intermittency in a warming world. *Geology*, **52**, 512–516.

McLeod, J.S., **Wood, J.**, **Lyster, S.J.**, **Valenza, J.M.**, **Spencer, A.R.T.** and **Whittaker, A.C.** (2023) Quantitative constraints on flood variability in the rock record. *Nat Commun*, **14**, 3362.

Meyer-Peter, E. and **Müller, R.** (1948) Formulas for Bed-Load transport.

Miall, A.D. (1994) Reconstructing fluvial macroform architecture from two-dimensional outcrops; examples from the Castlegate Sandstone, Book Cliffs, Utah. *Journal of Sedimentary Research*, **64**, 146–158.

Milliman, J.D. and **Meade, R.H.** (1983) World-Wide Delivery of River Sediment to the Oceans. *The Journal of Geology*, **91**, 1–21.

Molnar, P., **Anderson, R.S.**, **Kier, G.** and **Rose, J.** (2006) Relationships among probability distributions of stream discharges in floods, climate, bed load transport, and river incision. Journal of Geophysical Research: Earth Surface. doi: 10.1029/2005JF000310

Nijman, W. (1998) Cyclicity and basin axis shift in a piggyback basin: towards modelling of the Eocene Tremp-Ager Basin, South Pyrenees, Spain. *SP*, **134**, 135–162.

Nijman, W. and **Nio, S.D.** (1975) The Eocene Montañana Delta: Tremp-Graus Basin, Provinces of Lérida and Huesca, Southern Pyrenees, N. Spain). *Vakgroep Sedimentologie, Rijksuniveriteit Leiden-Utrecht*, 20 pp.

Nijman, W. and **Puigdefàbregas, C.** (1977) Coarse-Grained Point Bar Structure in a Molasse-Type Fluvial System, Eocene Castisent Sandstone Formation, South Pyrenean Basin.

Paola, C. and **Borgman, L.** (1991) Reconstructing random topography from preserved stratification. *Sedimentology*, **38**, 553–565.

Parker, G. (1976) On the cause and characteristic scales of meandering and braiding in rivers. *Journal of Fluid Mechanics*, **76**, 457–480.

Peucker-Ehrenbrink, B. (2009) Land2Sea database of river drainage basin sizes, annual water discharges, and suspended sediment fluxes. Geochemistry, Geophysics, Geosystems. doi: 10.1029/2008GC002356

Picart, J., **Samso, J.**, **Cuevas, J.L.**, **Mercade, L.** and **Arbues, P.** (2010) Mapa Geologic de Catalunya 1:2500. Espills 251-2-2 (64-22).

Piras, M., **Mascaro, G.**, **Deidda, R.** and **Vivoni, E.R.** (2016) Impacts of climate change on precipitation and discharge extremes through the use of statistical downscaling approaches in a Mediterranean basin. *Science of The Total Environment*, **543**, 952–964.

Plink-Bjorklund, P. (2015) Morphodynamics of rivers strongly affected by monsoon precipitation: Review of depositional style and forcing factors. Sedimentary Geology. doi: 10.1016/j.sedgeo.2015.04.004

Plint, A.G. and **Nummedal, D.** (2000) The falling stage systems tract: recognition and importance in sequence stratigraphic analysis. *Geological Society, London, Special Publications*, **172**, 1–17.

Prieur, M., **Robin, C.**, **Braun, J.**, **Vaucher, R.**, **Whittaker, A.C.**, **Jaimes-Gutierrez, R.**, **Wild, A.**, **McLeod, J.S.**, **Malatesta, L.**, **Fillon, C.**, **Schlunegger, F.**, **Sømme, T.O.** and **Castelltort, S.** (2025) Climate Control on Erosion: Evolution of Sediment Flux From Mountainous Catchments During a Global Warming Event, PETM, Southern Pyrenees, Spain. *Geophysical Research Letters*, **52**, e2024GL112404.

Puig, J.M., **Cabello, P.**, **Howell, J.** and **Arbués, P.** (2019) Three-dimensional characterisation of sedimentary heterogeneity and its impact on subsurface flow behaviour through the braided-to-meandering fluvial deposits of the Castissent Formation (late Ypresian, Tremp-Graus Basin, Spain). *Marine and Petroleum Geology*, **103**, 661–680.

Rezwan, N., **Whittaker, A.C.**, **McLeod, J.S.**, **Hook, J.**, **Castelltort, S.** and **Schlunegger, F.** (2025) Decoding Normal-Fault Controlled Trends in Stratigraphic Grain Size: Examples From the Kerinitis Gilbert-Type Delta, Greece. *Basin Research*, **37**, e70014.

Romans, B.W., **Castelltort, S.**, **Covault, J.A.**, **Fildani, A.** and **Walsh, J.P.** (2016a) Environmental signal propagation in sedimentary systems across timescales. *Earth-Science Reviews*, **153**, 7–29.

Romans, B.W., **Castelltort, S.**, **Covault, J.A.**, **Fildani, A.** and **Walsh, J.P.** (2016b) Environmental signal propagation in sedimentary systems across timescales. *Earth-Science Reviews*, **153**, 7–29.

Rowley, T., **Konsoer, K.**, **Langendoen, E.J.**, **Li, Z.**, **Ursic, M.** and **Garcia, M.H.** (2021) Relationship of point bar morphology to channel curvature and planform evolution. *Geomorphology*, **375**, 107541.

Rush, A.W.D., **Kiehl, A.J.T.**, **Shields, A.C.A.** and **Zachos, A.J.C.** (2021) Increased frequency of extreme precipitation events in the North Atlantic during the PETM: Observations and theory.

Selley, R.C. (1968) A Classification of Paleocurrent Models. *The Journal of Geology*, **76**, 99–110.

Sharma, N., **Whittaker, A.C.**, **Watkins, S.E.**, **Valero, L.**, **Vérité, J.**, **Puigdefabregas, C.**, **Adatte, T.**, **Garcés, M.**, **Guillocheau, F.** and **Castelltort, S.** (2023) Water discharge variations control fluvial stratigraphic architecture in the Middle Eocene Escanilla formation, Spain. *Sci Rep*, **13**, 6834.

Tramblay, Y. and **Somot, S.** (2018) Future evolution of extreme precipitation in the Mediterranean. *Climatic Change*, **151**, 289–302.

Trampush, S.M., **Huzurbazar, S.** and **McElroy, B.** (2014) Empirical assessment of theory for bankfull characteristics of alluvial channels. *Water Resources Research*, **50**, 9211–9220.

Turner, S.K. (2018) Constraints on the onset duration of the Paleocene-Eocene Thermal Maximum. *Philos Trans A Math Phys Eng Sci*, **376**, 20170082.

Van der Meulen, S. (1989) The distribution of Pyrenean erosion material, deposited by eocene sheetflood systems and associated fan-deltas : a fossil record in the Monllobat and adjacent Castigaleu formations, in the drainage area of the present Rio Noguerra Ribagorzana, provinces of Huesca and Lérida, Spain. *Rijksuniversiteit, Mineralogisch-geologisch instituut*, Utrecht, 125 pp.

Van Eden, J.G. (1970) A reconnaissance of deltaic environment in the middle Eocene of the south-central Pyrenees, Spain, 4th edn. *GEOL. EN MIJNBOUW*.

Wang, B. and **Ding, Q.** (2008) Global monsoon: Dominant mode of annual variation in the tropics. *Dynamics of Atmospheres and Oceans*, **44**, 165–183.

Wentworth, C.K. (1922) A Scale of Grade and Class Terms for Clastic Sediments. *The Journal of Geology*, **30**, 377–392.

Westerhold, T., `MarwanNorbert`, **Drury, A.J.**, **Liebrand, D.**, **Agnini, C.**, **Anagnostou, E.**, **Barnet, J.**, **Bohaty, S.**, **De Vleeschouwer, D.**, **Fabio, F.**, **Frederichs, T.**, **Hodell, D.**, **Holbourn, A.**, **Kroon, D.**, **Lauretano, V.**, **Littler, K.**, **Lourens, L.**, **Lyle, M.**, **Pälike, H.** and **Zachos, J.C.** (2020) An astronomically dated record of Earth's climate and its predictability over the last 66 million years. *Science (New York, N.Y.)*, **369**, 1383–1387.

Westerhold, T., **Röhl, U.**, **Donner, B.** and **Zachos, J.C.** (2018) Global Extent of Early Eocene Hyperthermal Events: A New Pacific Benthic Foraminiferal Isotope Record From Shatsky Rise (ODP Site 1209). *Paleoceanography and Paleoclimatology*, **33**, 626–642.

Westerhold, T., **Röhl, U.**, **Frederichs, T.**, **Agnini, C.**, **Raffi, I.**, **Zachos, J.C.** and **Wilkens, R.H.** (2017) Astronomical calibration of the Ypresian timescale: implications for seafloor spreading rates and the chaotic behavior of the solar system? *Climate of the Past*, **13**, 1129–1152.

Westra, S., **Fowler, H.J.**, **Evans, J.P.**, **Alexander, L.V.**, **Berg, P.**, **Johnson, F.**, **Kendon, E.J.**, **Lenderink, G.** and **Roberts, N.M.** (2014) Future changes to the intensity and frequency of short-duration extreme rainfall: FUTURE INTENSITY OF SUB-DAILY RAINFALL. *Rev. Geophys.*, **52**, 522–555.

Whitchurch, A.L., **Carter, A.**, **Sinclair, H.D.**, **Duller, R.A.**, **Whittaker, A.C.** and **Allen, P.A.** (2011) Sediment routing system evolution within a diachronously uplifting orogen: Insights from detrital zircon thermochronological analyses from the South-Central Pyrenees. *American Journal of Science*, **311**, 442–482.

Whittaker, A.C. (2012) How do landscapes record tectonics and climate? *Lithosphere*, **4**, 160–164.

Winnick, M.J., **Caves, J.K.** and **Chamberlain, C.P.** (2015) A mechanistic analysis of early Eocene latitudinal gradients of isotopes in precipitation. *Geophysical Research Letters*, **42**, 8216–8224.

Wolman, M.G. (1954) A method of sampling coarse river-bed material. *Eos, Transactions American Geophysical Union*, **35**, 951–956.

Wood, J., **McLeod, J.S.**, **Lyster, S.J.** and **Whittaker, A.C.** (2025) Reply to comment on 'Rivers of the Variscan Foreland: fluvial morphodynamics in the Pennant Formation of South Wales, UK.' *Journal of the Geological Society*, **182**, jgs2025-087.

Wood, J., **McLeod, J.S.**, **Lyster, S.J.** and **Whittaker, A.C.** (2022) Rivers of the Variscan Foreland: fluvial morphodynamics in the Pennant Formation of South Wales, UK. *Journal of the Geological Society*, **180**, jgs2022-048.

TABLES

Parameter	Definition

h_{xs}	Mean cross-set height, measured as the mean from a distribution of heights measured within one cross-set
h_d	Height of the original dune, before preservation as a cross-set
h_{acc}	Height of observable accretion set within preserved barforms
H	The depth of formative water flow at the time of deposition, often assumed to represent bankfull conditions
$q_{s,w}$	Unit discharge of water or sediment at the time of deposition, measured per unit width
$Q_{s,w}$	Discharge of water of sediment, measured per individual river channel
$Q_{s,w(total)}$	Total discharge of water or sediment for all channels of the river

1040 Table 1. Key palaeohydrological variables and definitions

	Number of barforms accreting downstream ($\Delta_{db} \leq 45°$)	Number of barforms accreting laterally ($45° < \Delta_{db} \leq 135°$)	Number of barforms accreting upstream ($\Delta_{db} > 135°$)
Castissent	45 (74%)	14 (23%)	2 (3%)
Montllobat	15 (39%)	17 (45%)	6 (16%)

1041 Table 2. Bar-mode results from dune-bar orientation difference analysis.

1042 **FIGURES**

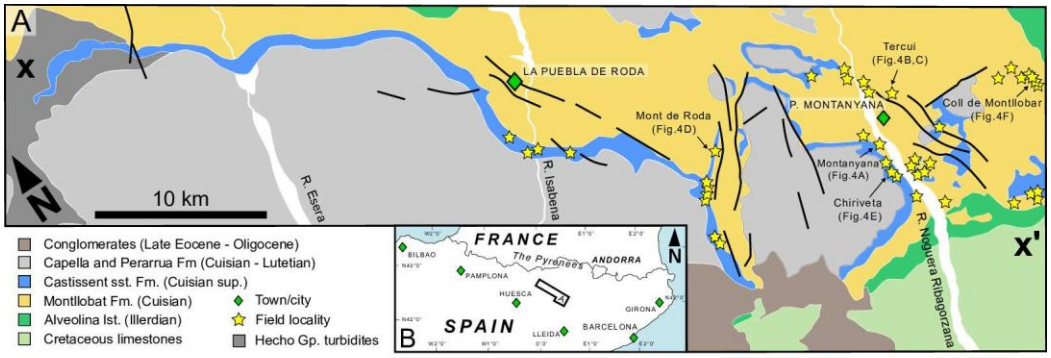

1043

1044 Fig 1. Study region. (A) Geologic map of field area and the Montllobat and Castissent
1045 Formations, including field localities (after Chanvry et al., 2018). Section X-X' is presented on
1046 Fig. 3. (B) Regional map, where the box is inset A.

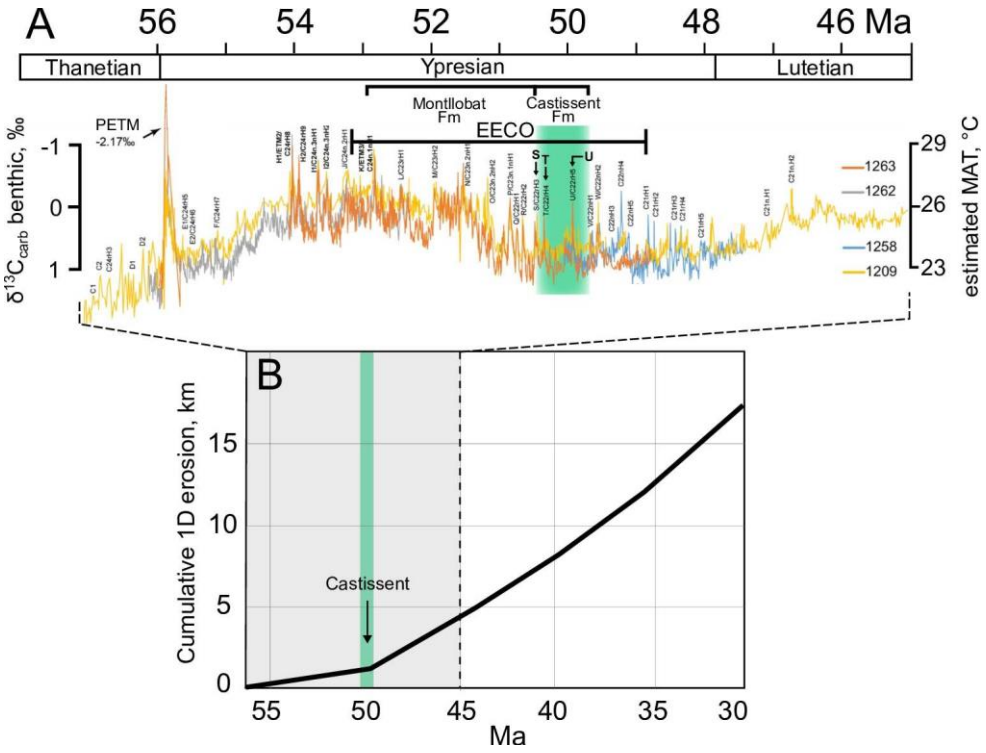

1047

1048 Fig 2. Tectono-climatic context of the Montllobat and Castissent Formations. (A) Benthic
1049 carbon isotope records for the upper Palaeocene and early Eocene (Honegger et al., 2020)
1050 where each coloured line represents δ13C from the IODP cores numbered on the right, and
1051 geologic timescale, with the Castissent interval highlighted in green. The mean annual
1052 temperature (MAT) change is illustrated with the axis on the right, estimated based on CO_2
1053 output (Honegger et al., 2020). (B) Cumulative 1-D erosion in Zone 4 of the Pyrenean orogen
1054 (Curry et al., 2021), illustrating exhumation from 56 – 30 Ma.

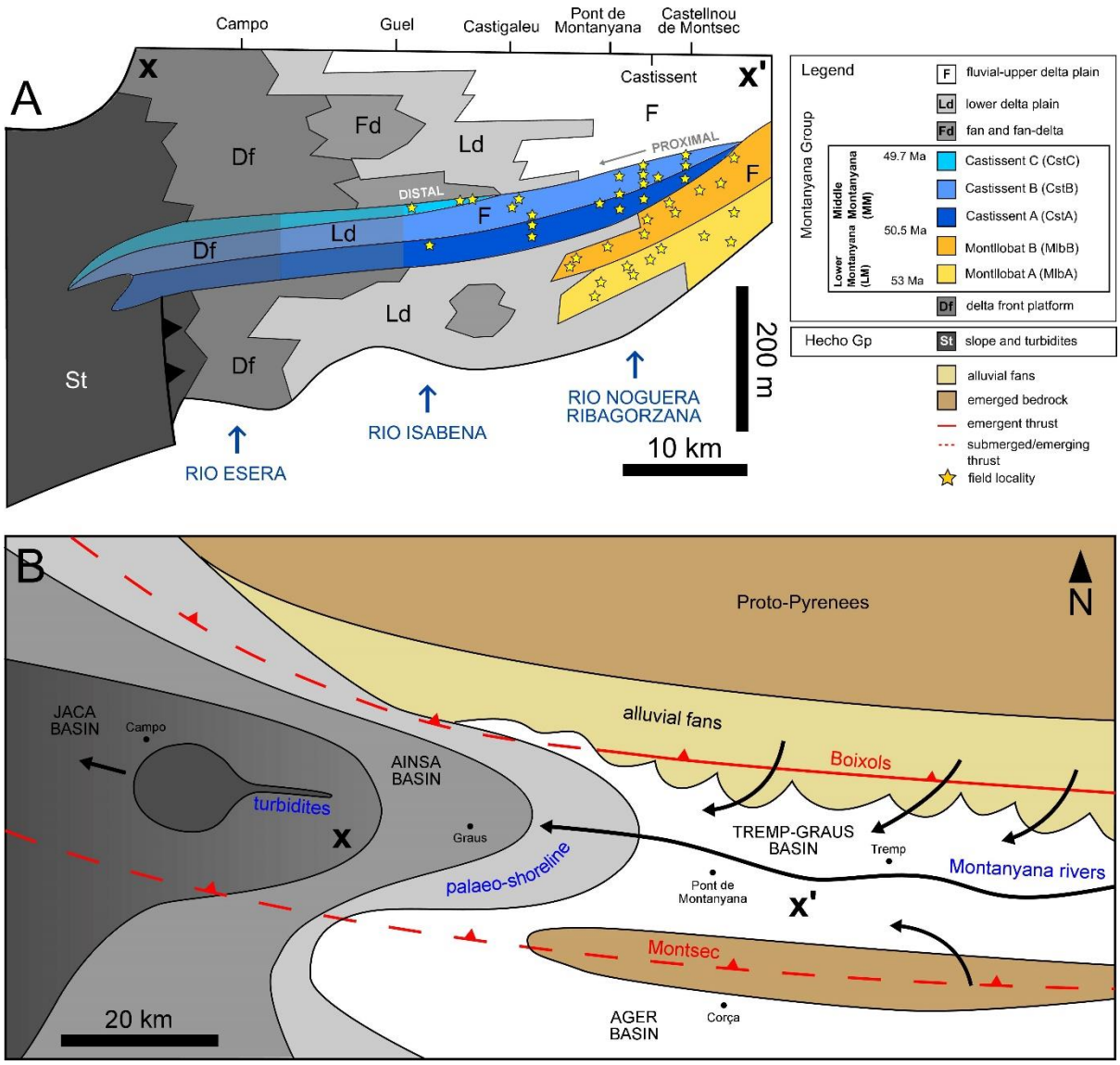

Fig 3. Stratigraphy and palaeogeography. (A) Schematic stratigraphic section, modified from Marzo (1988), from east (up-dip, X') to west (down-dip, X), showing field localities, major towns and rivers, and depositional environments. The location of section is labelled on Fig. 1A and Fig. 3B. (B) Schematic palaeogeographic map of the Montanyana sediment routing system c. 53-50 Mya, illustrating foreland sub-basins and depositional environments.

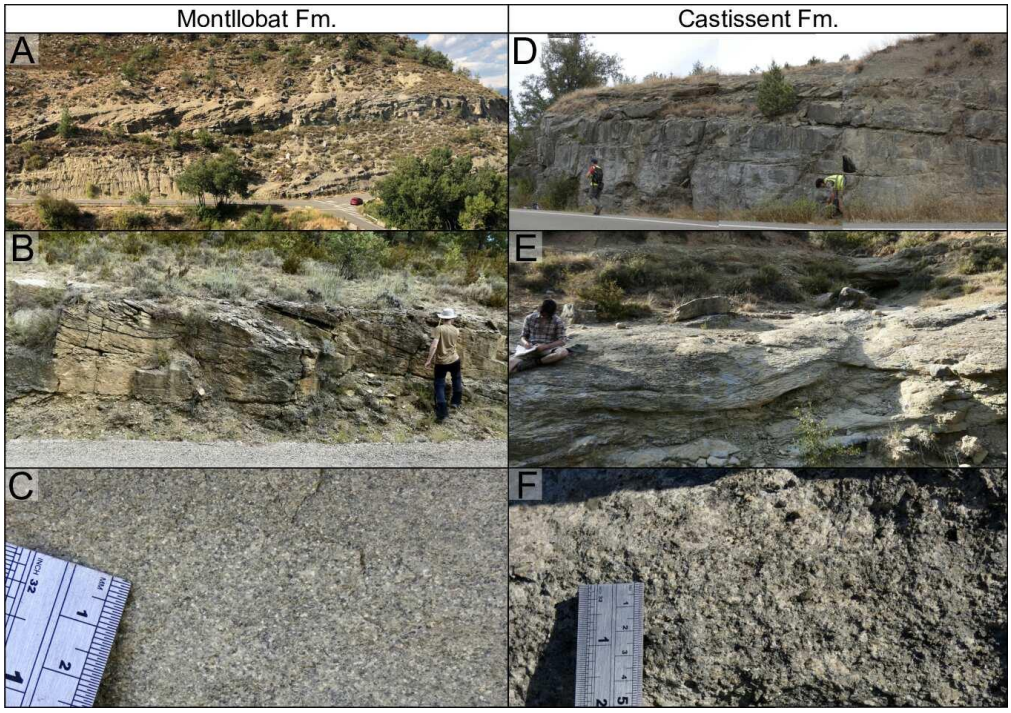

Fig. 4. The Montllobat (A-C) and Castissent (D-F) Formations at outcrop. (A) Point bar accretion sets at El Point Bar de Montanyana, (B) dune and bar-scale cross-strata near Tercui, (C) fine- to medium-grained sandstone near Tercui, (D) Amalgamated channel-fill sandstone bodies at Mont de Roda, (E) dune and bar-scale cross-strata at Chiriveta, (F) very coarse-grained sandstone near Coll de Montllobar. Locations shown on Fig. 1A.

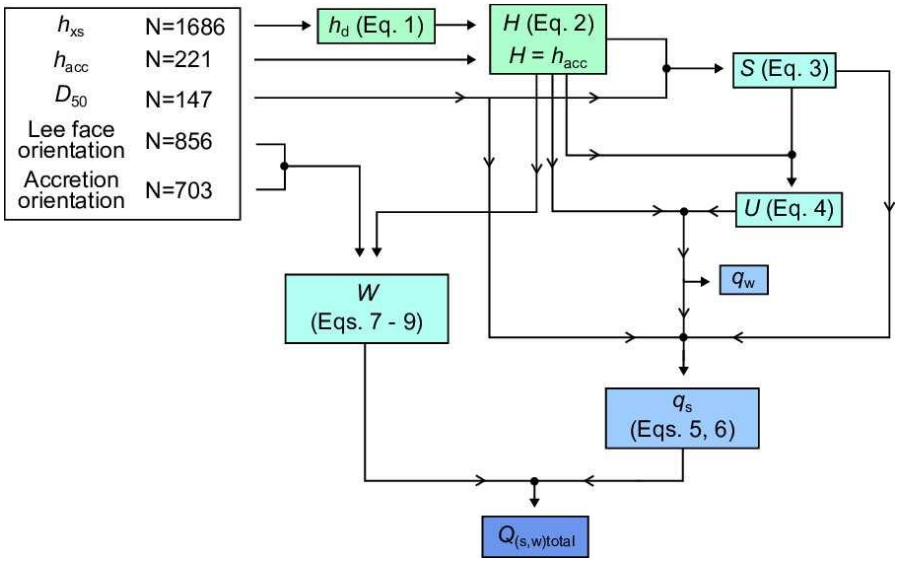

Fig. 5. Palaeohydrological workflow, from field data collection to quantitative suite of palaeohydrological approaches, where formulae used are indicated in each box. See Table 1 for definitions.

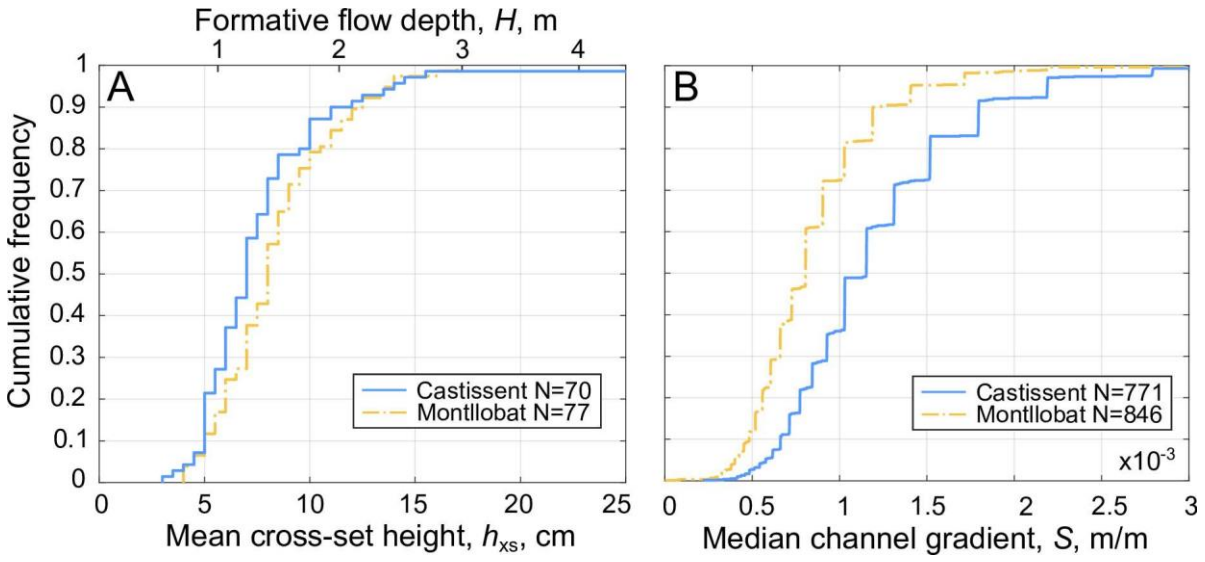

1071

1072 Fig. 6. Cumulative density functions (CDFs) of palaeohydrologic results. (A) CDF of mean
1073 cross-set thickness, and flow depth (calculated using Eqs. 1 and 2). (B) CDF of median channel
1074 gradient, *S*, calculated using Eq. 3.

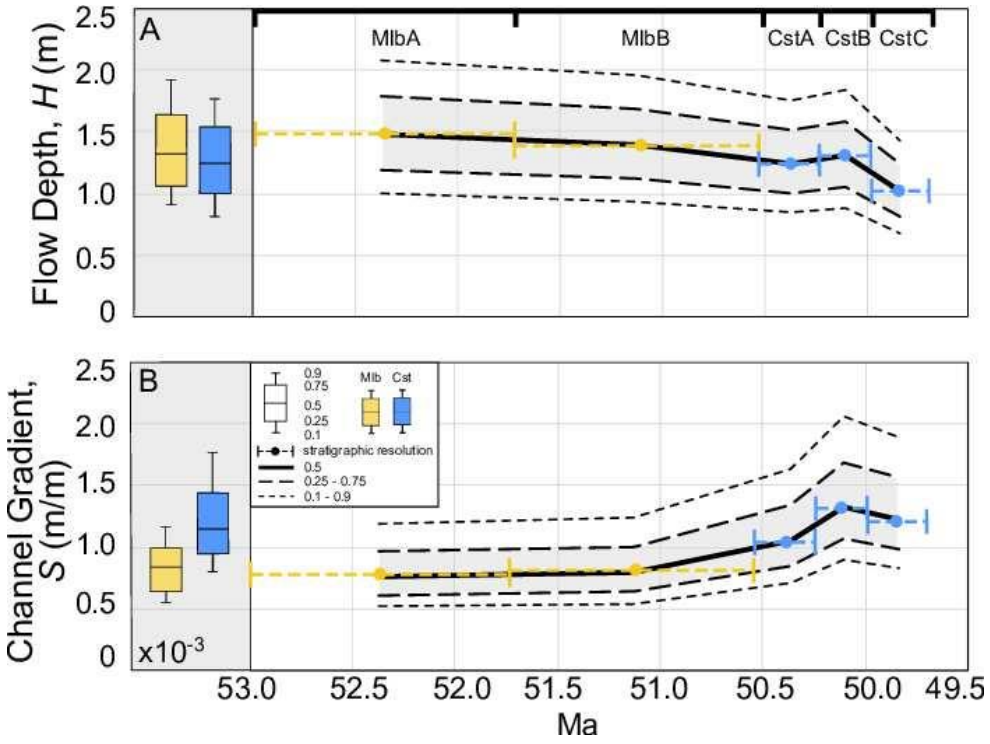

1075

1076 Fig. 7. Depth and slope through time. (A) Formative flow depth (bedform approach) through
1077 time. The box plots illustrate the reconstructed flow depth across each Formation, and the graph
1078 depicts uncertainty in reconstructed depth for each Member of the two Formations. Each
1079 Formation has been divided equally into its Members, as timing of their constituent fluvial
1080 deposits is poorly constrained. The solid black line represents the median value of flow depth,

the thick dashed lines represent the upper and lower quartiles (where the shaded region is the interquartile range), and the thin dashed lines represent the 10th and 90th percentiles. (B) As in (A) but for reconstructed palaeoslope.

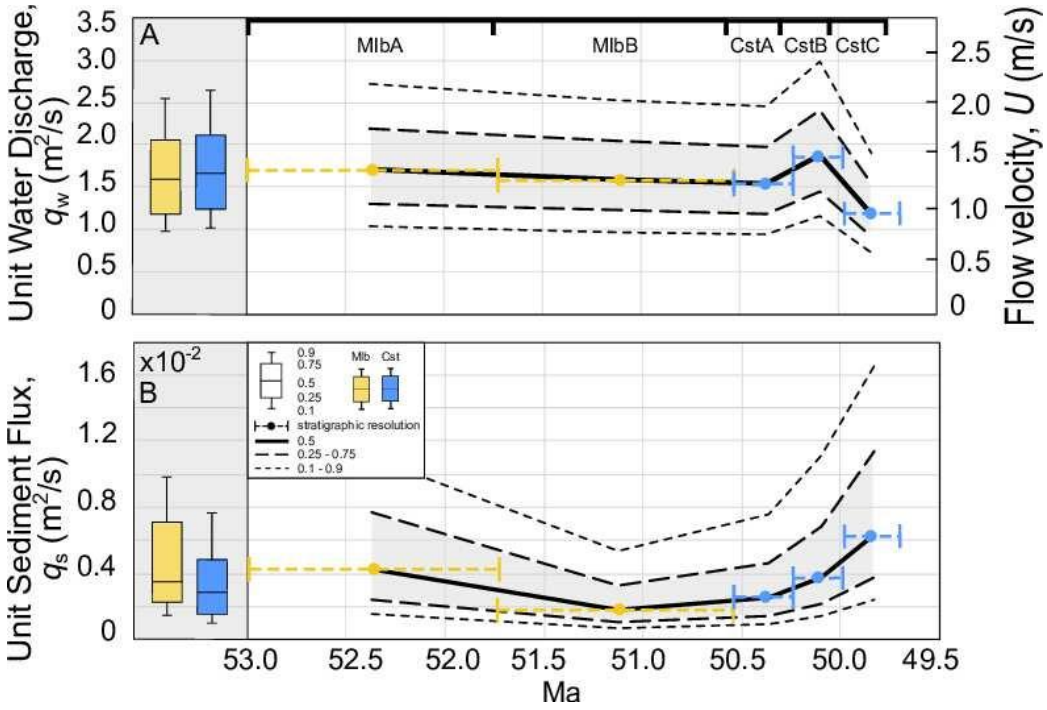

Fig. 8. Water and sediment discharge through time. (A) Unit water discharge, q_w, and flow velocity, U, through time, calculated using Eq. 4. The box plots represent the median depth within each Formation, and the graph depicts uncertainty in reconstructed q_w for each Member. The solid black line represents the median value, the thick dashed lines represent the upper and lower quartiles (where the shaded region is the interquartile range), and the thin dashed lines represent the 10th and 90th percentiles. (B) As in (A) but for reconstructed unit sediment flux, using Eq. 5.

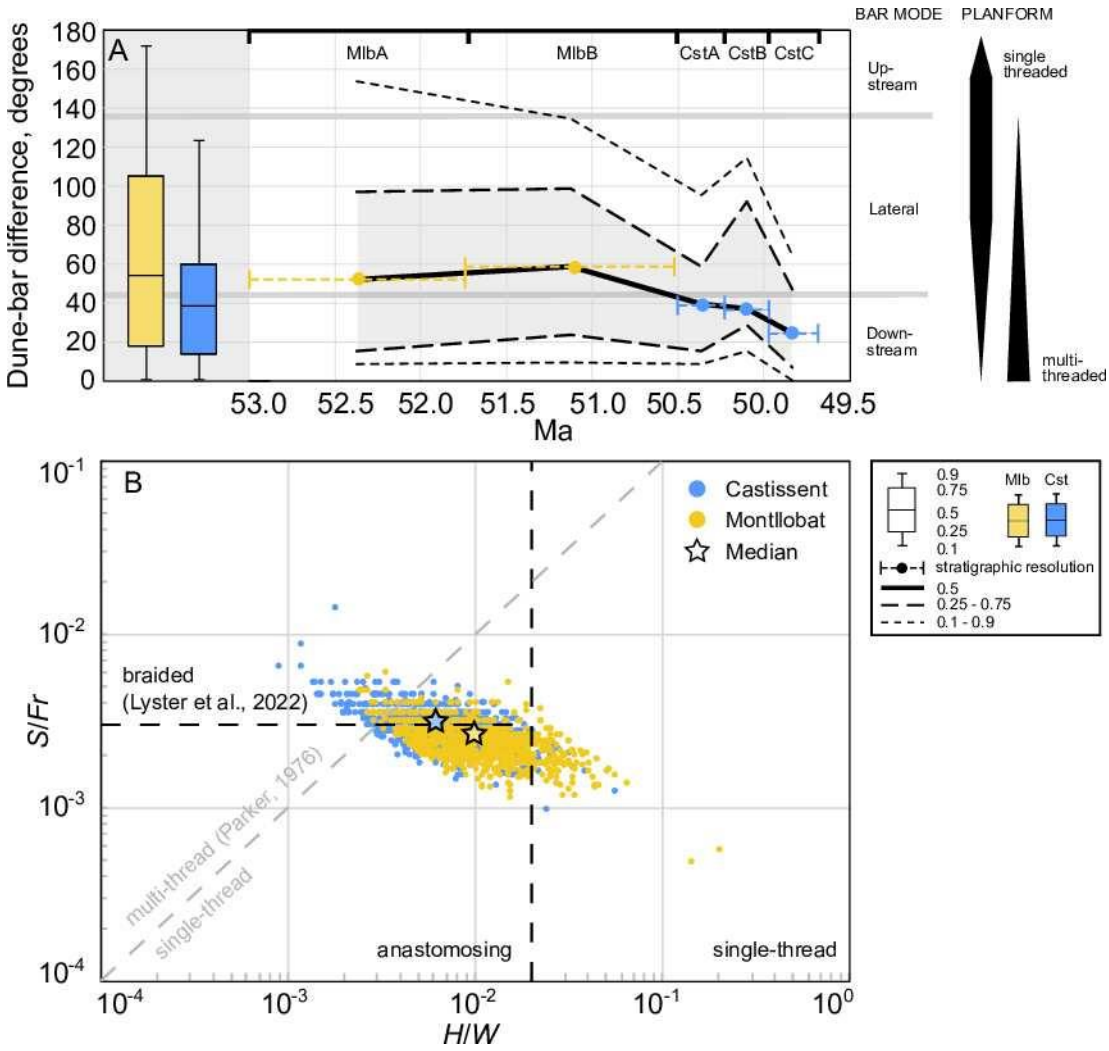

Fig. 9. Planform results. (A) Dune-bar angular difference through time, where the box plots represent the median dune-bar difference within each Formation, and the graph depicts uncertainty for each Member. Where median dune-bar angular difference is between 45 and 135°, dominant bar mode is considered to be lateral. The solid black line represents the median value, the thick dashed lines represent the upper and lower quartiles (where the shaded region is the interquartile range), and the thin dashed lines represent the 10th and 90th percentiles. (B) Planform stability plot, where slope/Froude number is plotted against depth/width, using a random distribution of values within uncertainty for each Formation. The planform stability fields of Parker (1976) and Lyster et al. (2022) are presented in grey and black, respectively.

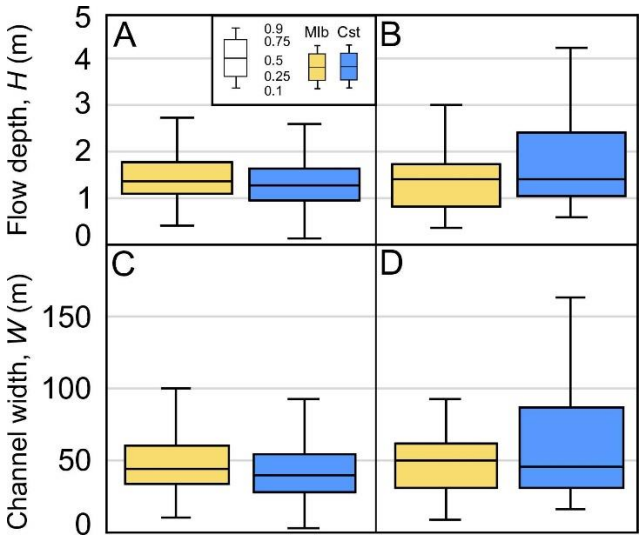

1102

1103 Fig. 10. Barform and bedform-based estimates of depth and width. (A) Boxplots illustrating
1104 flow depth results from the bedform approach, and (B) from the barform approach. (C) Channel
1105 width estimates (Eq. 8) using depths from the bedform approach, and (D) from the barform
1106 approach. Median width and depth values are comparable for each approach.

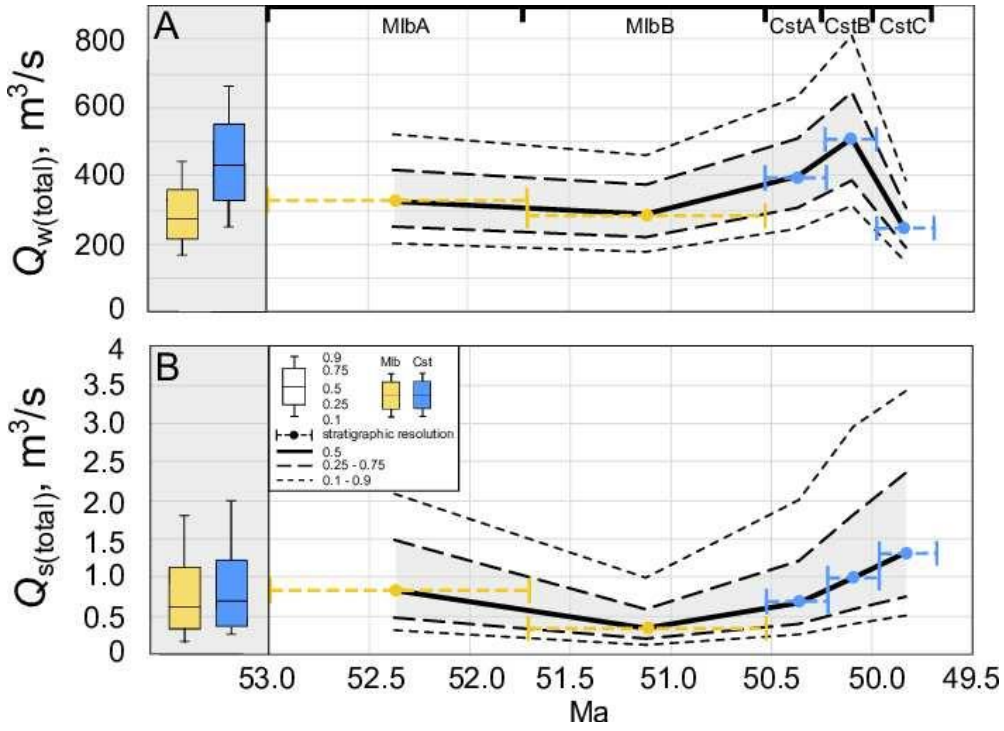

1107

1108 Fig 11. Total fluxes. (A) The total water discharge, $Q_{w(total)}$, and (B) the total sediment discharge,
1109 $Q_{s(total)}$. The solid black line represents the median value, the thick dashed lines represent the
1110 upper and lower quartiles (where the shaded region is the interquartile range), and the thin
1111 dashed lines represent the 10th and 90th percentiles.

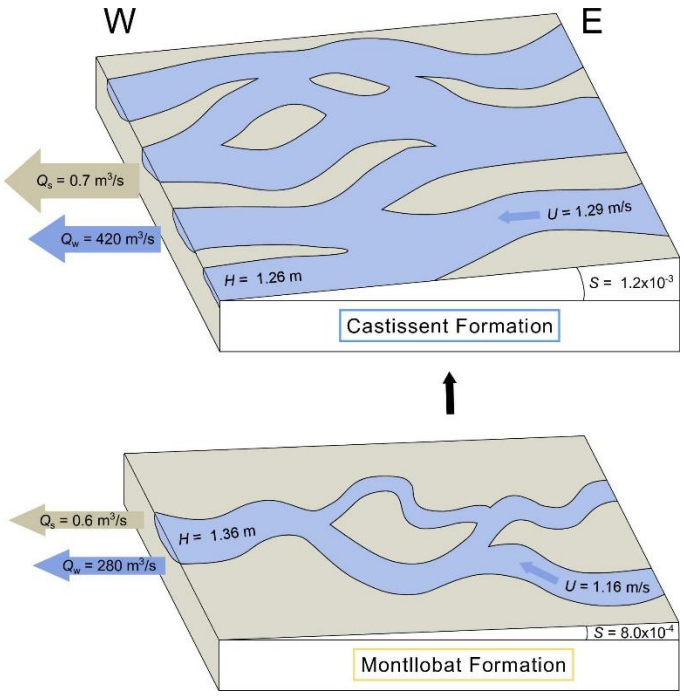

Fig. 12. Schematic diagram illustrating changing palaeoslope, flow velocity, depth, planform, and total water and sediment flux from the Montllobat to the Castissent Formation. Some values are not to scale.